Experimental/Theoretical Studies of the Paramagnetic 52/53-Electron Triangular Metal $[Ni_3(\eta^5\text{-}C_5H_5)_3(\mu_3\text{-}S)_2]^n$ Series (n = 1+, 0) Containing Weak Metal–Metal Bonding Interactions: Fenske–Hall MO Analysis of the Trimetal-Antibonding Frontier Orbitals Involved in the Reversible Redox-Generated Change in Ni_3S_2 Core Geometry

Terry E. North,[1a,b] James B. Thoden,[1a,c] Brock Spencer,[1d] and Lawrence F. Dahl*,[1a]

Departments of Chemistry, University of Wisconsin–Madison, Madison, Wisconsin 53706, and Beloit College, Beloit, Wisconsin 53511

Received October 5, 1992

In order to resolve the controversial nature of the metal–metal interactions in the frontier MOs as well as to discriminate between two proposed electronic ground states for the structurally known 53-electron S,S-bicapped $Ni_3Cp_3(\mu_3\text{-}S)_2$ (1) (where Cp denotes $\eta^5\text{-}C_5H_5$), the oxidative synthesis of its $[Ni_3Cp_3(\mu_3\text{-}S)_2]^+$ monocation (1^+) as the $[SbF_6]^-$ salt was carried out. $1^+[SbF_6]^-$, which was obtained by oxidation of 1 with $[FeCp_2]^+[SbF_6]^-$, was characterized by a single-crystal X-ray diffraction analysis, and 1 and 1^+ were characterized by comparative spectroscopic (^{1}H NMR, IR, UV–vis), mass spectrometric, cyclic voltammetric, variable-temperature magnetic susceptibility, and molecular orbital (MO) studies. From a valence-bond viewpoint, the 53-electron 1 is electronically unique in possessing five valence electrons more than the 48 needed for a metal triangle with three single bonds. Its previously determined crystal-twinned "averaged structure" of crystallographic C_{3h} site symmetry contains a regular trigonal-bipyramidal Ni_3S_2 core with a cyclopentadienyl ring coordinated to each nickel atom; the observed long Ni–Ni distance of 2.801(5) Å was originally attributed to the five valence electrons being trimetal-antibonding such that the weakly attractive metal–metal interactions are due to one net bonding electron. A subsequent Fenske–Hall MO investigation showed that the five valence electrons in 1 occupy three nearly degenerate a_2' and e′ HOMOs under D_{3h} symmetry; it was then proposed that 1 has either a $^2A_2'$ ($e'^4a_2'^1$) or $^2E'$ ($a_2'^2e'^3$) ground state and that the e′ HOMOs of 1 are *trimetal-bonding* in opposition to the earlier experimentally-based bonding model. The room-temperature X-ray crystallographic investigation of $1^+[SbF_6]^-$ revealed a crystal-ordered C_{2v} Ni_3S_2 core geometry consisting of an isosceles nickel triangle with one nonbonding edge of 3.145(2) Å and two bonding edges of 2.536(2) Å. From a valence-bond formalism the total net metal–metal bond order of 1.0 for the 52-electron 1^+ (presumed to have four *trimetal-antibonding* valence electrons) must be equally distributed between the two Ni–Ni bonding edges to give an individual bond order of $^1/_2$ corresponding to a net 1-electron metal–metal bond. The only salient bond-length change in the Ni_3S_2 core upon oxidation of 1 to 1^+ is the 0.06 Å shorter mean Ni–Ni distance of 2.74 Å in 1^+, which is consistent with the removal of the unpaired electron from a *trinickel-antibonding* HOMO of 1. MO calculations performed on 1 and 1^+ via the nonparameterized Fenske–Hall model are correlated with the experimental data. These new theoretically-based results contradict the previously published Fenske–Hall MO interpretation in indicating that the e′ HOMOs as well as the a_2' HOMO of 1 (and the corresponding two HOMOs of 1^+) are trimetal-antibonding; hence, these new MO results are also in agreement with the original experimentally-based valence-bond predictions for electron-rich trimetal clusters containing valence electrons in excess of 48. Furthermore, the near-degeneracy in the two half-occupied, nondegenerate b_1 and a_1 HOMOs obtained from the MO calculations for the C_{2v} geometry of the 52-electron 1^+ is consistent with the observed room-temperature magnetic moment in both the solid state (μ_{eff} = 2.8 μ_B via the Faraday method) and solution (μ_{eff} = 2.7 μ_B via the Evans NMR method) showing that 1^+ has two unpaired electrons at room temperature. Thus, the experimental data of 1^+ indicate that its ground state is $^3E'$ ($a_2'^1e'^3$) under D_{3h} symmetry and $^3B_1$ ($b_1^2b_1^1a_1^1$) under C_{2v} symmetry. $[Ni_3Cp_3(\mu_3\text{-}S)_2]^+[SbF_6]^-$: tetragonal, $a = b = 11.261(1)$ Å, $c = 16.234(2)$ Å, $P4_2/ncm$ with $Z = 4$.

Introduction

In 1968 Vahrenkamp, Uchtman, and Dahl[2] reported the synthesis of $S_2Ni_3(C_5H_5)_3$,[2] now formulated as $Ni_3Cp_3(\mu_3\text{-}S)_2$ (1), where Cp denotes $\eta^5\text{-}C_5H_5$, and its characterization by X-ray crystallographic, infrared, and solution magnetic susceptibility measurements. Although the X-ray dif-

(1) (a) University of Wisconsin—Madison. (b) Present address: Molecular Design Ltd., Parsippany, NJ 07054. (c) Present address: Institute for Enzyme Research, University of Wisconsin—Madison. (d) Beloit College.

0276-7333/93/2312-1299$04.00/0

fraction analysis of the crystal structure of 1 was complicated by a crystal-twinning of its hexagonal unit cell, its structure was solved by the application of a twinning model developed by Wei.[3] The molecular geometry of 1 of crystallographic C_{3h}-3/m site symmetry consists of an equilateral nickel triangle capped on each side by a sulfur atom with a cyclopentadienyl ring coordinated to each nickel atom. This S,S-bicapped triangular nickel cluster is of particular interest in possessing a unique electronic configuration (vide infra) and an unusually long independent Ni–Ni distance (2.801(5) Å) which is 0.41 Å greater than that found[4] in the crystal-ordered D_{3h} $Ni_3(CO)_2$ core of the structurally analogous Fischer–Palm $Ni_3Cp_3(\mu_3\text{-}CO)_2$ molecule.[5] In order to rationalize the abnormally long Ni–Ni distance in 1, Vahrenkamp et al.[2] proposed from a valence-bond formalism that the assumption of no Ni–Ni bonding results in the entire molecule being one electron short of a closed-shell electronic configuration for each nickel and that this conceptual representation, if correct, immediately suggests the probable addition of an electron to give the $[S_2Ni_3(C_5H_5)_3]^-$ anion. They further speculated on the basis of qualitative MO symmetry arguments that, with one unpaired electron in the highest energy antibonding level, the Ni–Ni interactions are effectively due to the net difference of only one electron in a strongly bonding metal symmetry orbital and that it is expected that the Ni–Ni interactions are weak in agreement with the long identical Ni–Ni distances. They also stated that an obvious implication is that electrons can be selectively removed to give cationic species with considerably shorter Ni–Ni bonds. Subsequent cyclic voltammetric measurements in benzonitrile by Madach and Vahrenkamp[6] in 1981 indicated that 1 undergoes a reversible 1-electron oxidation to give the monocation and a reversible 1-electron reduction to give the monoanion.

These bonding predictions concerning the dominant influence of trimetal-antibonding valence electrons on the metal–metal bonds in 1 were soon substantiated by structural/magnetic studies[7-10] on other X,Y-bicapped $M_3Cp_3(\mu_3\text{-}X)(\mu_3\text{-}Y)$ clusters. In 1972 it was pointed out[9] that variations in mean metal–metal distances are in accordance with a bonding model[2,11] which assumes five antibonding electrons for $Ni_3Cp_3(\mu_3\text{-}S)_2$ (2.80 Å), two antibonding electrons for $Co_3Cp_3(\mu_3\text{-}S)_2$ (2.69 Å),[7-9] one antibonding electron for the $[Co_3Cp_3(\mu_3\text{-}S)_2]^+$ monocation as the iodide salt (2.59 Å),[9] and no antibonding electrons for $Co_3Cp_3(\mu_3\text{-}S)(\mu_3\text{-}CO)$ (2.45 Å).[9] The 0.1 Å longer Co–Co distance in $Co_3Cp_3(\mu_3\text{-}S)(\mu_3\text{-}CO)$ compared to that in the electronically equivalent $Co_3Cp_3(\mu_3\text{-}O)(\mu_3\text{-}CO)$ (2.37 Å)[10] was readily attributed[9] to the influence of the larger (and less electronegative) triply bridging sulfur ligand. Our recent bonding description of 1 as a 53-electron system, the $[Co_3Cp_3(\mu_3\text{-}S)_2]^n$ series (n = 0, 1+) as 50/49-electron systems, and $Co_3Cp_3(\mu_3\text{-}X)(\mu_3\text{-}CO)$ (X = S, O) as 48-electron systems is based upon our utilization[12] of the Lauher rule (proposed[13,14] in 1978) to bookkeep the observed number of cluster valence electrons (CVEs) for these trimetal clusters.

Our interest in $Ni_3Cp_3(\mu_3\text{-}S)_2$ (1) was renewed by the MO investigation reported in 1982 by Rives, You, and Fenske[15] via the parameter-free Fenske–Hall model[16] on 1 and related bicapped triangular metal clusters. Their calculations showed that the five valence electrons in excess of the 48 electrons necessary for a complete metal–metal-bonded Ni_3S_2 core in 1 occupy three frontier MOs consisting (under presumed D_{3h} symmetry) of two closely spaced levels of a_2' and e' symmetry (with the doubly degenerate e' MOs being only 0.3 eV higher in energy than the a_2' MO). Consequently, they proposed that 1 possesses either a nondegenerate $^2A_2'$ ($e'^4a_2'^1$) or a degenerate $^2E'$ ($a_2'^2e'^3$) ground state; on account of the a_2' level being energetically lower, they favored the latter $^2E'$ state, which should cause a first-order Jahn–Teller geometrical distortion that would remove the 3-fold molecular symmetry. Because the 3d Ni AOs of 1 are contracted as well as separated at long distances, they further suggested that any Jahn–Teller distortion of the $^2E'$ state of the nickel triangle would expectedly be small. Thus, the true individual molecular geometry of 1 plays a vital role in any experimental probe used to determine its electronic ground state. Unfortunately, the crystallographic C_{3h} site symmetry imposed on the independent $Ni_3Cp_3(\mu_3\text{-}S)_2$ molecule gives rise to a 3-fold-averaged molecular structure, which thereby masks any possible distortions of the Ni_3S_2 core in an individual molecule toward C_{2v} symmetry.

In addition, from their MO calculations Rives et al.[15] proposed that the e' HOMOs of 1 are primarily composed of *trimetal-bonding* interactions. This prediction completely contradicts the systematic "experimental quantum mechanical" studies[2,4b,9-11,17] (outlined above), which indicate that any valence electrons in excess of electron-pair bonds in a completely bonding triangular metal cluster (i.e., greater than a valence electron count of 48) occupy *antibonding* metal symmetry orbitals. In this connection, the a_2' MO was experimentally and theoretically shown to be trimetal-antibonding, initially from structural/ESR investigations of 49-electron $Co_3(CO)_9(\mu_3\text{-}X)$ (where X = S, Se)[11] and 49-electron $Ni_3Cp_3(\mu_3\text{-}CO)_2$[4b,17] (both of which possess an unpaired electron in the a_2' HOMO) and subsequently from the MO calculations by Rives et al.[15] on 1 as well as on the 50-electron $Co_3Cp_3(\mu_3\text{-}S)_2$ and 49-

(2) Vahrenkamp, H.; Uchtman, V. A.; Dahl, L. F. *J. Am. Chem. Soc.* **1968**, *90*, 3272–3273.
(3) (a) Wei, C. H.; Wilkes, G. R.; Dahl, L. F. *J. Am. Chem. Soc.* **1967**, *89*, 4792–4793. (b) Wei, C. H. *Inorg. Chem.* **1969**, *8*, 2384–2397.
(4) (a) Hock, A. A.; Mills, O. S. In *Advances in the Chemistry of Coordination Compounds*; Kirschner, S., Ed.; Macmillan: New York, 1961; pp 640–648. (b) Byers, L. R.; Uchtman, V. A.; Dahl, L. F. *J. Am. Chem. Soc.* **1981**, *103*, 1942–1951.
(5) Fischer, E. O.; Palm, C. *Chem. Ber.* **1958**, *91*, 1725–1731.
(6) Madach, T.; Vahrenkamp, H. *Chem. Ber.* **1981**, *114*, 505–512.
(7) (a) Otsuka, S.; Nakamura, A.; Yoshida, T. *Inorg. Chem.* **1968**, *7*, 261–265. (b) Otsuka, S.; Nakamura, A.; Yoshida, T. *Justus Liebigs Ann. Chem.* **1968**, *719*, 54–60.
(8) Sorai, M.; Kosaki, A.; Suga, H.; Seki, S.; Yoshida, T.; Otsuka, S. *Bull. Chem. Soc. Jpn.* **1971**, *44*, 2364–2371.
(9) (a) Frisch, P. D.; Dahl, L. F. *J. Am. Chem. Soc.* **1972**, *94*, 5082–5084. (b) Frisch, P. D. Ph.D. Thesis, University of Wisconsin—Madison, 1972.
(10) Uchtman, V. A.; Dahl, L. F. *J. Am. Chem. Soc.* **1969**, *91*, 3763–3769.
(11) (a) Strouse, C. E.; Dahl, L. F. *Discuss. Faraday Soc.* **1969**, No. 47, 93–106. (b) Strouse, C. E.; Dahl, L. F. *J. Am. Chem. Soc.* **1971**, *93*, 6032–6041.
(12) Kharas, K. C. C.; Dahl, L. F. *Adv. Chem. Phys.* **1988**, *70* (Part 2), 1–43.
(13) In 1978 Lauher[14] formulated an electron-counting scheme for transition metal clusters based upon extended Hüeckel calculations. Lauher[14] showed from an interaction diagram for a completely bonding trimetal cluster that three of the 27 MOs formed from the 9 valence AOs per metal atom are high-lying empty antibonding orbitals (HLAOs) while the other 24 MOs, which he termed as cluster valence molecular orbitals (CVMOs), are filled. The vast majority of triangular metal organometallic clusters possess 48 cluster valence electrons (CVEs) corresponding from a valence-bond viewpoint to three electron-pair metal–metal bonds.
(14) Lauher, J. W. *J. Am. Chem. Soc.* **1978**, *100*, 5305–5315.
(15) Rives, A. B.; You, X.-Z.; Fenske, R. F. *Inorg. Chem.* **1982**, *21*, 2286–2294.
(16) (a) Hall, M. B.; Fenske, R. F. *Inorg. Chem.* **1972**, *11*, 768–775. (b) Fenske, R. F. *Prog. Inorg. Chem.* **1976**, *21*, 179–208. (c) Fenske, R. F. *Pure Appl. Chem.* **1971**, *27*, 61–71.
(17) Maj, J. J.; Rae, A. D.; Dahl, L. F. *J. Am. Chem. Soc.* **1982**, *104*, 3054–3063.

electron $Ni_3Cp_3(\mu_3\text{-}CO)_2$. Thus, Rives et al.[15] concluded from the Fenske–Hall MO calculations that the frontier MOs of the 53-electron $Ni_3Cp_3(\mu_3\text{-}S)_2$ contain three trimetal-bonding and two trimetal-antibonding electrons instead of five trimetal-antibonding electrons.

Since their theoretically-based conclusion is completely contrary to our previous experimentally-based predictions, the research presented here had two intertwined objectives: (1) to determine experimentally whether it is possible to assign the electronic ground state of 1 as $^2A_2'$ or $^2E'$ and, if the latter, to deduce whether its 3-fold molecular geometry is significantly perturbed by a Jahn–Teller vibronically-induced distortion; (2) to isolate the methylcyclopentadienyl analogue of 1 and/or the monocation and monoanion of 1 (whose existences are indicated from the electrochemical study[6]) in the hope that structural/magnetic analyses would allow one to obtain persuasive support for the validity of our electron-counting formalism which assumes that the frontier e′ MOs as well as the a_2' MO possess trimetal-antibonding orbital character.

Initial work involved the preparation of the methylcyclopentadienyl $Ni_3Cp'_3(\mu_3\text{-}S)_2$ (2) (where Cp′ denotes η^5-C_5H_4Me) in which noncylindrical Cp′ ligands were substituted for cylindrical Cp ones in order to increase the likelihood that the Cp′-containing 2 would crystallize without imposed C_{3h} symmetry and would thereby permit an unambiguous structural determination of its actual geometry. This same approach has been successfully employed in the preparation and structural characterization of the crystal-ordered Cp′-containing 49-electron $Co_3Cp'_3(\mu_3\text{-}NO)(\mu_3\text{-}NH)$,[18] which provided convincing evidence that the unpaired electron occupies a doubly degenerate e HOMO (under C_{3v} symmetry) rather than a nondegenerate a_2 HOMO in that a markedly distorted isosceles metal triangle characteristic of a Jahn–Teller induced distortion was observed. The desired product (2) was obtained from the reaction of $Ni_2Cp'_2(\mu_2\text{-}CO)_2$ with elemental sulfur. However, purification of 2 has proved to be difficult, and attempts to grow crystals suitable for X-ray diffraction measurements have been unsuccessful. Efforts to prepare 2 by use of CS_2 as the source of sulfur resulted instead in the isolation of the Fischer–Palm analogue $Ni_3Cp'_3(\mu_3\text{-}CO)_2$ and the related 49-electron thiocarbonyl-capped $Ni_3Cp'_3(\mu_3\text{-}CS)(\mu_3\text{-}CO)$ and $Ni_3Cp'_3(\mu_3\text{-}CS)_2$ as three major products[19] and $[Ni_3Cp'_3]_2(C_2S_6)$, which contains the unprecedented hexathioethane ligand, $C_2S_6^{6-}$, as a minor product.[20]

We then decided to pursue a structural-bonding investigation of the 52-electron monocation and 54-electron monoanion of 1 because changes of the Ni–Ni distances in these species would probably yield experimental evidence regarding the nature of the metal–metal interactions present in the frontier orbitals and, in addition, the geometry of the 52-electron monocation would hopefully indicate the electronic ground state of 1 as well as that of 1^+. Redox syntheses of the monocation and the monoanion from the neutral 1 were undertaken. The $[SbF_6]^-$ salt of the 52-electron $[Ni_3Cp_3(\mu_3\text{-}S)_2]^+$ monocation (1^+) was prepared and crystallized; however, attempts to prepare the 54-electron monoanion have not been successful to date. Reported herein are the details of the oxidative synthesis of $[Ni_3Cp_3(\mu_3\text{-}S)_2]^+$ (1^+) as the $[SbF_6]^-$ salt and a characterization of its physical behavior by X-ray crystallographic, spectroscopic, cyclic voltammetric, and solution and solid-state magnetic susceptibility studies. An improved high-yield synthesis of the known $Ni_3Cp_3(\mu_3\text{-}S)_2$ (1) is also presented along with a further investigation of its physical properties. MO calculations were performed via the Fenske–Hall method[16] on both 1 and 1^+ to obtain a valid comparative theoretical analysis by use of the same atomic basis functions, which differ somewhat from those used by Rives et al.[15] in their Fenske–Hall MO analysis of 1 (vide infra). The MO results are correlated with the geometries and experimental data obtained for 1 and 1^+.

Recently, Pulliam et al.[21] reported the structural-bonding analysis of the 50/49/48-electron methylcyclopentadienyl $[Co_3Cp'_3(\mu_3\text{-}S)_2]^n$ series (n = 0, 1+, 2+). Their observation of a significant shortening of the mean Co–Co distance upon successive removal of the two "excess" valence electrons from the highly bent C_{2v} Co_3S_2 core geometry in the neutral 50-electron $Co_3Cp'_3(\mu_3\text{-}S)_2$ parent is clearly incompatible with the theoretical interpretation given by Rives et al.[15] that the orbital nature of the e′ HOMO is trimetal-bonding in the corresponding cyclopentadienyl $[Co_3Cp_3(\mu_3\text{-}S)_2]^n$ series (n = 0, 1+, 2+), for which only the neutral parent (n = 0) and its monocation (n = 1+) had been crystallographically characterized. Pulliam et al.[21] proposed that the metal–metal bond-length variations could be correlated with the results of the Fenske–Hall MO calculations on the basis that the e′ HOMOs exert a trimetal-antibonding influence on the geometries of these electron-rich triangular metal clusters due to the importance of the more diffuse Co 4s and $4p_z$ AOs; it was presumed that their minor trimetal-antibonding contributions to the frontier e′ HOMOs dominate over the major trimetal-bonding in-plane Co $3d_{xz}$ contributions due to much better orbital overlap at long metal–metal distances. Most notably, the current Fenske–Hall MO calculations presented herein on 1 and 1^+ contradict the theoretically-based conclusion reached by Rives et al.[15] concerning the trimetal-orbital nature of the e′ HOMOs in 1; an examination of the Ni–Ni orbital overlap populations indicates that both the occupied e′ and a_2' frontier orbitals (under D_{3h} symmetry) in 1 and 1^+ are trimetal-antibonding and that the orbital interactions in the e′ HOMOs involve 3d Ni AOs as well as the 4s and 4p Ni AOs. These theoretically-based results are of prime importance in indicating that the Fenske–Hall MO bonding description is indeed in harmony with our original experimentally-based valence-bond description in providing a general foundation for recent electron-counting schemes[12] which predict for electron-rich triangular metal clusters that CVEs in excess of 48 are trimetal-antibonding. Details of the orbital overlap population analysis (obtained from the Fenske–Hall MO calculations) that led to this current interpretation are reported herein.

Experimental Section

General Techniques and Materials. Work was done with rigorous exclusion of air and water. All reactions and manipulations were carried out under an atmosphere of nitrogen that had been dried by passage through an Aquasorb column.

(18) Bedard, R. L.; Dahl, L. F. *J. Am. Chem. Soc.* **1986**, *108*, 5942–5948.

(19) North, T. E.; Thoden, J. B.; Spencer, B.; Bjarnason, A.; Dahl, L. F. *Organometallics* **1992**, *11*, 4326–4337.

(20) North, T. E.; Thoden, J. B.; Bjarnason, A.; Dahl, L. F. *Organometallics* **1992**, *11*, 4338–4343.

(21) Pulliam, C. R.; Thoden, J. B.; Stacy, A. M.; Spencer, B.; Englert, M. H.; Dahl, L. F. *J. Am. Chem. Soc.* **1991**, *113*, 7398–7410.

Standard Schlenk-type apparatus and techniques were employed, either with a preparative vacuum line or a Vacuum Atmospheres drybox. The following solvents were dried and freshly distilled under N_2 prior to use: acetone ($CaCO_3$), acetonitrile (CaH_2), carbon disulfide (CaH_2), cyclopentane (Na, anthracene), dichloromethane (CaH_2), hexane (CaH_2), THF (K, benzophenone), and toluene (Na). Anhydrous ether and benzene were used as received. All deuterated NMR solvents were predried over activated 3-Å molecular sieves, frozen and degassed three times, and then vacuum-distilled before use. $Ni_2Cp_2(\mu_2\text{-}CO)_2$ and $Ni_2Cp'_2(\mu_2\text{-}CO)_2$ were prepared by the method of King[22] from reaction of nickel tetracarbonyl with nickelocene or bis(methylcyclopentadienyl)nickel, respectively, in refluxing benzene. The two nickelocenes used for the above reactions were synthesized by the method of Cordes.[23] $[FeCp_2]^+[SbF_6]^-$ was prepared by the method of Carney et al.[24] except that dichloromethane was used as the solvent instead of petroleum ether. Kryptofix 222 (2,2,2-crypt) and K-Selectride (potassium tri-*sec*-butylborohydride) were obtained from Aldrich and used as received. All other reagents were purchased from major suppliers and used without further purification.

Syntheses. (a) Preparation of $Ni_3Cp_3(\mu_3\text{-}S)_2$ (1). $Ni_3Cp_3(\mu_3\text{-}S)_2$ was prepared via a modification of the synthesis reported by Vahrenkamp.[2] A 1-equiv sample of elemental sulfur (0.28 g, 8.79 mmol) was slowly added to a stirring ether solution containing 2.00 g (6.59 mmol) of $Ni_2Cp_2(\mu_2\text{-}CO)_2$. The reaction was allowed to continue for 12 h, during which time the color of the solution changed from red to brown. Filtration gave a black precipitate. The desired product was obtained in 85% yield from this precipitate by extraction with CH_2Cl_2 and subsequent recrystallization from ether at −78 °C.

(b) Preparation of $[Ni_3Cp_3(\mu_3\text{-}S)_2]^+[SbF_6]^-$. In a typical reaction, 0.9 equiv of $[FeCp_2]^+[SbF_6]^-$ (260 mg, 0.62 mmol) was slowly added as a CH_2Cl_2 slurry to a stirred solution of the neutral parent 1 (300 mg, 0.69 mmol) in CH_2Cl_2 at −78 °C. The reaction mixture was allowed to warm to room temperature and then stirred for another 3 h. The oxidized product was isolated by repeated extraction of the reaction mixture with CH_2Cl_2. After removal of the solvent under vacuum, the extracts were washed with toluene to remove ferrocene and any residual neutral parent (1). The monocation (1^+) was obtained as a black crystalline powder in ca. 60% yield.

(c) Preparation of $Ni_3Cp'_3(\mu_3\text{-}S)_2$ (2). In a typical reaction, 1 equiv of elemental sulfur (0.13 g, 4.00 mmol) was slowly added to a stirring hexane solution containing 1.00 g (3.00 mmol) of $Ni_2Cp'_2(\mu_2\text{-}CO)_2$. The color of the solution quickly changed from red to brown. Gas evolution, which was presumably due to the rapid generation of carbon monoxide, was observed if all the sulfur was added at once. The reaction was allowed to continue for 12 h at room temperature, after which the hexane-soluble material was removed and discarded. The precipitate was then separated into two fractions, first by removing an acetone extract and then by removing a CH_2Cl_2 extract from the residue. Mass spectra of powder samples from both extracts gave a parent ion peak of m/z 477 along with the expected trinickel isotope pattern for $Ni_3Cp'_3(\mu_3\text{-}S)_2$. Numerous attempts to further purify and grow suitable crystals of this methylcyclopentadienyl analogue of 1 for an X-ray diffraction investigation were unsuccessful.

(d) Attempted Preparation of $[K(2,2,2\text{-crypt})]^+[Ni_3Cp_3(\mu_3\text{-}S)_2]^-$. In a typical reaction, 0.20 mL of a 1 M solution of K-Selectride (0.20 mmol of K^+) was slowly syringed into a −78 °C CH_2Cl_2 solution containing 100 mg (0.23 mmol) of $Ni_3Cp_3(\mu_3\text{-}S)_2$ (1). The stirred solution was allowed to warm to room temperature after 10 min. The reaction was allowed to continue for 0.5 h, after which 130 mg (0.345 mmol) of Kryptofix 222 was added and the solution was stirred for another 0.5 h. The very dark green CH_2Cl_2 solution was then filtered away from an insoluble black residue. A brown precipitate was obtained by adding toluene to the CH_2Cl_2 solution. Unfortunately, this brown precipitate was highly unstable and quickly decomposed during further attempts at purification and recrystallization. No further investigation of this reaction has been carried out.

Characterization of $Ni_3Cp_3(\mu_3\text{-}S)_2$ (1) and $[Ni_3Cp_3(\mu_3\text{-}S)_2]^+$ (1^+). (a) Physical Properties. Both compounds are black crystalline powders as solids and both form very dark red-brown solutions. Compound 1 is relatively air-stable in the solid state but slowly decomposes in solution. It is soluble in toluene, CH_2Cl_2, and THF but only slightly soluble in ether, acetone, and CH_3CN. The $[SbF_6]^-$ salt of 1^+ is moderately air-sensitive in the solid state and is relatively unstable in solution. It is soluble in the polar solvents THF and acetone and slightly soluble in CH_3CN and CH_2Cl_2.

(b) Infrared Data. Infrared data were collected with a Mattson Instruments Polaris FT-IR spectrophotometer. Solid-state infrared spectra (KBr pellet) of 1 and the $[SbF_6]^-$ salt of 1^+ show bands characteristic of π-bonded cyclopentadienyl rings. The vibrational frequencies of the μ_3-S ligands were beyond the spectral range of the instrument used. Symmetric and asymmetric Ni–S stretching modes of 1 have been assigned by Oxton and co-workers[25] to bands occurring at 282 and 272 cm^{-1}, respectively. In addition, an IR spectrum of $1^+[SbF_6]^-$ revealed an intense band at 659 cm^{-1}, corresponding to a vibrational mode of the $[SbF_6]^-$ anion.[26]

(c) NMR Data. Proton NMR data were recorded on a Bruker WP270 or WP200 FT-NMR spectrometer. Shifts were referenced indirectly to TMS via residual proton signals in the deuterated solvent. Sweep widths of ±300 ppm were employed when paramagnetically shifted lines were searched for. Low-intensity signals were observed with two instruments (200 and 270 MHz) and with different spectral windows to eliminate the possibility of "fold-over" signals from outside the spectral window and to detect artifacts.

Proton NMR measurements of 1 in $CDCl_3$ showed a broad paramagnetically shifted resonance of low intensity at δ −111 ppm due to the cyclopentadienyl ring protons. The line width was approximately 690 Hz at baseline. Proton NMR measurements of $1^+[SbF_6]^-$ in acetone-d_6 also displayed a broad paramagnetically shifted cyclopentadienyl proton resonance at δ −82 ppm. The line width was approximately 1300 Hz at the baseline.

(d) ESR Data. Spectra at room temperature and at 130 K were recorded on a Varian E-15 ESR spectrometer. Glass samples were prepared by rapidly quenching dilute solutions in liquid nitrogen. ESR studies of 1 and $1^+[SbF_6]^-$ in CH_2Cl_2 solution at room temperature and as a CH_2Cl_2 glass at 130 K gave no detectable signals.

(e) Magnetic Susceptibility Data. Solid-state magnetic susceptibility measurements were performed via the Faraday method. Specific details of the instrumentation and method used are reported elsewhere.[27] Measurements were performed on three independently prepared samples for both 1 and $1^+[SbF_6]^-$ over a typical temperature range of 2–320 K. Data were obtained at three magnetic fields of 5.2, 15.8, and 19.5 kG at each temperature to determine the field dependence and check for ferromagnetic impurities. No field dependence was observed in the measured susceptibilities of either 1 or $1^+[SbF_6]^-$. The magnetic susceptibilities were corrected for the nickel and ligand diamagnetism. The values used for this correction were $\chi_M^{dia} = -390 \times 10^{-6}$ emu/mol for 1 and $\chi_M^{dia} = -470 \times 10^{-6}$ emu/mol for $1^+[SbF_6]^-$.[28]

(22) King, R. B. *Organometallic Synthesis*; Academic Press: New York, 1965; Vol. 1, pp 119–121.
(23) Cordes, J. F. *Chem. Ber.* **1962**, *95*, 3084–3085.
(24) Carney, M. J.; Lesniak, J. S.; Likar, M. D.; Pladziewicz, J. R. *J. Am. Chem. Soc.* **1984**, *106*, 2565–2569.
(25) (a) Oxton, I. A.; Powell, D. B.; Skinner, P.; Markó, L.; Werner, H. *Inorg. Chim. Acta* **1981**, *47*, 177–179. (b) Hempleman, A. J.; Oxton, I. A.; Powell, D. B.; Skinner, P.; Deeming, A. J.; Markó, L. *J. Chem. Soc., Faraday Trans. 2* **1981**, *77*, 1669–1679.
(26) Nyquist, R. A.; Kagel, R. O. *Infrared Spectra of Inorganic Compounds*; Academic Press: New York, 1971; p 393.
(27) Miller, J. S.; Dixon, D. A.; Calabrese, J. C.; Vazquez, C.; Krusic, P. J.; Ward, M. D.; Wasserman, E.; Harlow, R. L. *J. Am. Chem. Soc.* **1990**, *112*, 381–398.
(28) Mulay, L. N.; Boudreaux, E. A. *Theory and Applications of Molecular Diamagnetism*; Wiley: New York, 1976; pp 303–307.

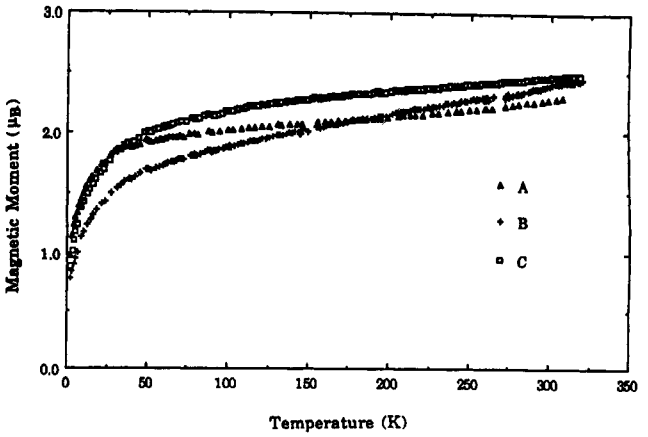

Figure 1. Magnetic moment as a function of temperature for three independently prepared samples (denoted as A, B, and C) of $Ni_3Cp_3(\mu_3\text{-}S)_2$ (1).

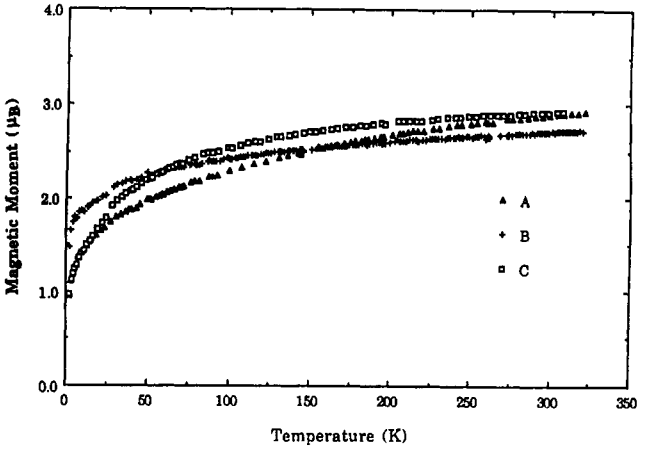

Figure 2. Magnetic moment as a function of temperature for three independently prepared samples (denoted as A, B, and C) of $[Ni_3Cp_3(\mu_3\text{-}S)_2]^+$ (1^+) as the $[SbF_6]^-$ salt.

Table I. Values of the Effective Magnetic Moment (μ_{eff}) and Weiss Constants (θ, K) for Three Independently Prepared Samples of $Ni_3Cp_3(\mu_3\text{-}S)_2$ (1) and $[Ni_3Cp_3(\mu_3\text{-}S)_2]^+$ (1^+) as the $[SbF_6]^-$ Salt[a]

	μ_{eff} @ 298K	μ	θ
1 (A)	2.30	1.88	−3.2
(B)	2.40	1.56	−2.5
(C)	2.46	2.21	−14
1^+ (A)	2.89	3.49	−138
(B)	2.70	2.94	−52
(C)	2.92	3.19	−59

[a] Weiss constants for 1 were obtained from a fit of the corrected data to the Curie–Weiss expression; Weiss constants for 1^+ were derived from the uncorrected data in the high-temperature region (T > 100 K).

The magnetic moments calculated from magnetic susceptibility measurements on 1 in the solid state are plotted versus temperature in Figure 1. Results from measurements made on the three independently prepared samples are designated A, B, and C. The corresponding results for the three samples of $1^+[SbF_6]^-$ are plotted in Figure 2. Values for μ_{eff} at 298 K are given in Table I. Representative inverse molar susceptibility (χ^{-1}) data corresponding to measurements on sample A are plotted versus temperature for both 1 and $1^+[SbF_6]^-$ in Figure 3. For each of the three samples of 1 measured, a similar nonlinear relationship between χ^{-1} and temperature was observed. An approximately linear plot was obtained by subtracting an empirically derived constant from the value of χ in each set of data. The magnitudes of the corrections employed were 700, 1400, and 600 × 10^{-6} emu/mol for samples A, B, and C, respectively. Values of μ (in units of μ_B) and the Weiss constants (θ, in Kelvin) obtained from a fit

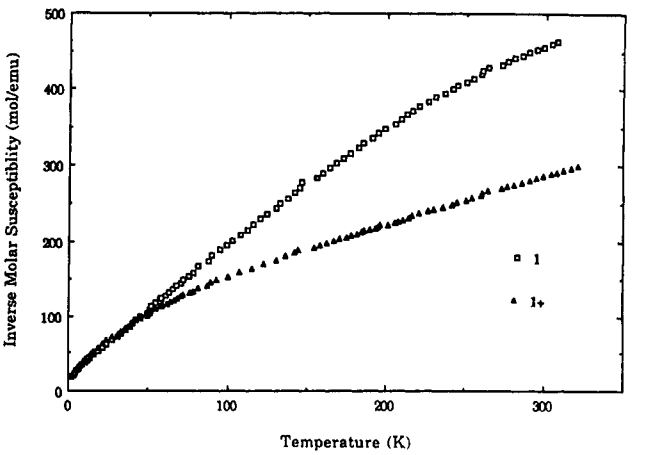

Figure 3. Representative plots of inverse molar magnetic susceptibility (mol/emu) versus temperature (K) for $Ni_3Cp_3(\mu_3\text{-}S)_2$ (1) and $[Ni_3Cp_3(\mu_3\text{-}S)_2]^+$ (1^+) as the $[SbF_6]^-$ salt.

of the corrected data to the Curie–Weiss expression,[29] $\chi = C/(T - \theta)$, are given in Table I. The corresponding values for $1^+[SbF_6]^-$ were derived from the uncorrected data in the high-temperature region (above 100 K), where χ^{-1} is linear in T without corrections applied to χ. In both compounds the Weiss constants were not used in the calculations of the effective moments.

Solution bulk magnetic susceptibility measurements on 1 via the Evans NMR technique[30] were previously carried out by Vahrenkamp et al.[2] who obtained μ_{eff} = 1.7 ± 0.3 μ_B at room temperature in accordance with one unpaired electron in solution. Solution bulk magnetic susceptibility measurements of $1^+[SbF_6]^-$ via the Evans NMR technique in deuterated acetone gave a temperature-independent magnetic moment of 2.7 ± 0.01 μ_B from room temperature (298 K) down to 205 K. A plot of the inverse molar susceptibility versus temperature is linear, indicating that the $[SbF_6]^-$ salt of 1^+ obeys the Curie–Weiss law over the 298–205 K range in solution. The temperature-independent magnetic moment calculated from the slope of the line is 2.66 μ_B and θ = +2 K. No correction was made for TIP (temperature-independent paramagnetism).

(f) UV–Vis Data. Room-temperature spectra were recorded in CH_2Cl_2 solution on a Hewlett Packard 8452A diode array spectrophotometer. Quartz sample cells of 0.1-cm path length were used; all spectra were corrected for the solvent background.

A UV–vis spectrum of 1 in the region between 190 and 820 nm exhibited one major broad band in the visible region at λ_{max} = 396 nm ($\epsilon \sim 10^3$ mol^{-1} cm^{-1}). Two additional UV bands were observed at 220 and 272 nm (Figure 4). A UV–vis spectrum of $1^+[SbF_6]^-$ in the same region displayed similar bands. The visible region exhibited a broad band at λ_{max} = 382 nm ($\epsilon \sim 10^3$ mol^{-1} cm^{-1}) with shoulders at ca. 320 and 450 nm. The two UV bands occurred at 220 and 264 nm (Figure 4).

(g) Mass Spectral Data. Mass spectra were obtained with an EXTREL FT-MS 2000 laser desorption Fourier transform (LD/FT) mass spectrometer.[31] Details of the instrumentation and procedures for sample preparation and data collection are found elsewhere.[32] Accurate mass determinations and isotopic

(29) The Curie constant, C, can be obtained from the χ^{-1} vs T plot by taking the reciprocal of the slope, (i.e., $\chi^{-1} = C^{-1}T$). From C the effective magnetic moment can be calculated from the equation $\mu_{eff} = (3k/N)^{1/2}(\chi T)^{1/2} = 2.823(C)^{1/2}$.

(30) (a) Evans, D. F. *Proc. Chem. Soc.* **1958**, 115–116. (b) Evans, D. F. *J. Chem. Soc.* **1959**, 2003–2005. (c) Fritz, H. P.; Schwarzhans, K.-E. *J. Organomet. Chem.* **1964**, *1*, 208–211. (d) Live, D. H.; Chan, S. I. *Anal. Chem.* **1970**, *42*, 791–792. (e) Crawford, T. H.; Swanson, J. *J. Chem. Educ.* **1971**, *48*, 382–386. (f) Ostfeld, D.; Cohen, I. A. *J. Chem. Educ.* **1972**, *49*, 829. (g) Gerger, W.; Mayer, U.; Gutmann, V. *Monatsh. Chem.* **1977**, *108*, 417–422.

(31) Mass spectral data were graciously collected by Dr. Robert Weller (Extrel FTMS, Madison WI).

(32) (a) Bjarnason, A.; DesEnfants, R. E., II; Barr, M. E.; Dahl, L. F. *Organometallics* **1990**, *9*, 657–661. (b) Bjarnason, A. *Rapid Commun. Mass Spectrom.* **1989**, *3*, 373–376.

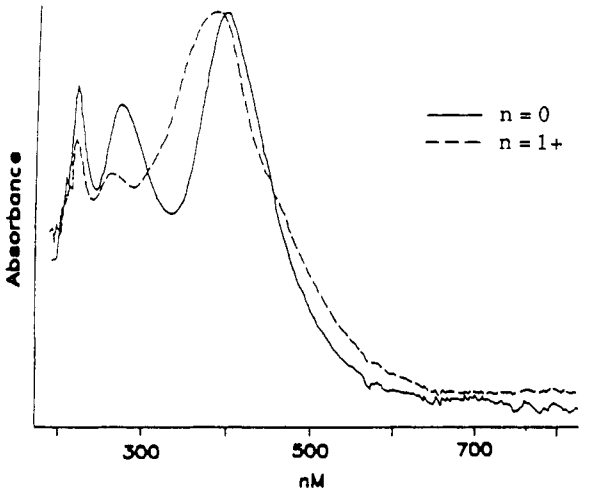

Figure 4. UV–vis spectra of the $[Ni_3Cp_3(\mu_3\text{-}S)_2]^n$ series (n = 0, 1+).

distribution patterns aided in the spectral analysis. Both positive- and negative-ion spectra were recorded for each sample.

The composition of 1 was confirmed from both the negative- and positive-ion mass spectra, which displayed the parent ion peak $[M]^{-,+}$. Major ion peaks (with their ion-fragment assignments and intensities relative to the base peak as 100 given in parentheses) obtained from the negative-ion spectrum are as follows: m/z 435 ($[M]^-$, 100), 403 ($[M - S]^-$, 25), 370 ($[M - 2S - H]^-$, 46), 370 ($[M - Cp]^-$, 36), and 305 ($[M - 2Cp]^-$, 22). The positive-ion spectrum displayed only two major peaks, viz., m/z 435 ($[M]^+$, 100) and 188 ($[NiCp_2]^+$, 45).

Mass spectra of 1^+ as the $[SbF_6]^-$ salt did not exhibit a parent cation peak. The positive-ion spectrum displayed only one major peak corresponding to the nickelocenium ion (m/z 188), while the negative-ion spectrum showed ion peaks due to the counterion, viz., $[SbF_6]^-$ (m/z 235), $[SbF_5]^-$ (m/z 216), and $[SbF_4]^-$ (m/z 197).

(h) Cyclic Voltammetric Data. Electrochemical measurements were performed on a BAS-100 electrochemical analyzer in conjunction with a Parr electrochemical cell operated inside a Vacuum Atmospheres drybox under an atmosphere of purified nitrogen. The three-electrode cell was composed of a platinum-disk working electrode, a platinum-wire counter electrode, and a saturated calomel electrode as a reference. A 0.1 M tetra-*n*-butylammonium hexafluorophosphate solution was used as the supporting electrolyte. Additional details of the cell configuration and experimental method are found elsewhere.[33] In each of the measurements presented, iR compensation was made for solution resistance, and linear sweep voltammetry (LSV) was used to verify the direction of electron transfer (oxidation or reduction). Half-wave potentials ($E_{1/2}$) were calculated as the mean potential between the peak potentials by use of the equation $E_{1/2} = (E_{pa} + E_{pc})/2$, where E_{pa} is the anodic peak potential and E_{pc} is the cathodic peak potential. Electrochemical reversibility was evidenced from both the near-unity values of the peak-current ratio (i_a/i_c) and the separation between anodic and cathodic peak potentials (ΔE_p) being nearly independent of scan rate.[34] Electrochemical data collected for 1 and 1^+ at a scan rate of 200 mV/s are summarized in Table II and Figure 5.

(i) Elemental Analysis. The stoichiometries of $Ni_3Cp_3(\mu_3\text{-}S)_2$ (1) and the $[SbF_6]^-$ salt of $[Ni_3Cp_3(\mu_3\text{-}S)_2]^+$ (1^+) are in agreement with the elemental analyses (Soils Laboratory, University of Wisconsin—Madison). Anal. Calcd (found) for $Ni_3S_2C_{15}H_{15}$ (1): Ni, 40.44 (40.02); S, 14.72 (14.58); C, 41.36 (39.98); H, 3.47 (3.29). For $SbF_6Ni_3S_2C_{15}H_{15}$: Ni, 26.24 (25.91); S, 9.55 (9.21); C, 26.84 (26.49); H, 2.25 (2.02).

(j) Nonparameterized Fenske–Hall Molecular Orbital Calculations. Calculations for 1 and 1^+ were performed with the Fenske–Hall molecular orbital model.[16] This nonparameterized model is based on a self-consistent-field method, which is an approximation of the Hartree–Fock–Roothaan procedure. The molecular geometry and the atomic basis sets used completely determine the resulting eigenvalues and eigenvectors. For 1 under D_{3h} symmetry (with presumed cylindrical Cp rings), the bond distances were Ni–Ni, 2.80 Å, Ni–S, 2.17 Å, and Ni–C(ring), 2.13 Å. For 1^+ under C_{2v} symmetry (which likewise presumes the Cp rings to be cylindrical), the bond distances were Ni–Ni, 2.536 and 3.145 Å, Ni–S, 2.19 Å (to the unique Ni atom on the C_2 axis) and 2.16 Å (to the other two Ni atoms), and Ni–C(ring), 2.12 Å. Basis functions[35] for neutral H, C, and S atoms were used.

Table II. Electrochemical Data for the $[Ni_3Cp_3(\mu_3\text{-}S)_2]^n$ Series (n = 0, 1+)[a]

solvent	redox step	$E_{1/2}$, V	ΔE_p, mV	i_{pa}/i_{pc}
		a. n = 0		
CH_2Cl_2	0 → 1+	+0.09	136	1.08
CH_2Cl_2	1+ → 2+	+0.97[b]		irrev
CH_2Cl_2	0 → 1−	−0.81	135	0.95
acetone	0 → 1+	−0.00	61	1.04
acetone	0 → 1−	−0.88	63	0.94
CH_3CN	0 → 1+	−0.02	88	1.06
CH_3CN	0 → 1−	−0.83	77	0.95
CH_3CN	oxid, n = ?	+1.05[b]		irrev
CH_3CN	oxid, n = ?	+1.30[b]		irrev
		b. n = 1+		
acetone	1+ → 0	0.00	61	0.95
acetone	0 → 1−	−0.87	58	0.89

[a] $E_{1/2}$ denotes the mean potential between the peak potentials E_{pa} and E_{pc}, ΔE_p is the difference between the two peak potentials, and i_{pa}/i_{pc} denotes the peak current ratio. All data are for a scan rate of 200 mV/s. [b] The value given for an irreversible oxidation is the anodic peak potential (E_{pa}).

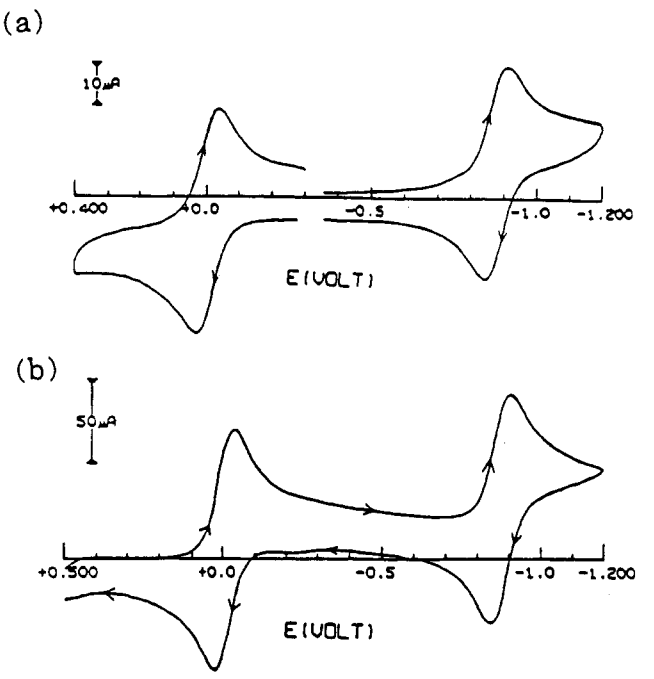

Figure 5. Comparison of cyclic voltammograms of (a) $Ni_3Cp_3(\mu_3\text{-}S)_2$ (1) and (b) $[Ni_3Cp_3(\mu_3\text{-}S)_2]^+$ (1^+) in acetone-d_6 at a scan rate of 200 mV/s. Arrows are placed on the plots to contrast the reversible one-electron oxidation and reduction of 1 in a to the corresponding two successive one-electron reductions of 1^+ in b.

(33) Bedard, R. L.; Dahl, L. F. *J. Am. Chem. Soc.* **1986**, *108*, 5933–5942.

(34) The experimental values of ΔE_p obtained from cyclic voltammograms of organometallic clusters are often larger than the theoretically determined value for a reversible couple (cf. ref 33 and references cited therein). Therefore, the magnitude of ΔE_p was not used as a criterion for electrochemical reversibility.

(35) Clementi, E.; Ramondi, D. L. *J. Chem. Phys.* **1963**, *38*, 2686–2689.

Table III. Crystal, Data Collection, and Refinement Parameters for $[Ni_3Cp_3(\mu_3\text{-}S)_2]^+[SbF_6]^-$

fw	671.30
cryst syst	tetragonal
$a = b$, Å	11.261(1)
c, Å	16.234(2)
vol, Å^3	2058.6(6)
space group	$P4_2/ncm$
Z	4
d_{calcd}, g/cm^3	2.17
temp, °C	20
μ, cm^{-1}	42.7
scan mode	ω
2θ limits, deg	3.0–45.0
scan speed, deg/min	variable; 3.0–29.3
background analysis	profile
no. check refl/freq	3/47
no. of data collcd	2710 in 1 octant
no. of ind data, $\|F\| > 3\sigma(F)$	980
no. params refined	76
data/param ratio	12.9/1
$R(F)$,[a] $R_w(F)$[b]	4.71%, 6.14%
GOF[c]	1.36

[a] $R(F) = R_1(F) = [\sum(\|\|F_o\| - \|F_c\|\|)/\sum(|F_o|)] \times 100$. [b] $R_w(F) = R_2(F) = [\sum w_i(\|\|F_o\| - \|F_c\|\|)^2/\sum w_i(|F_o|)^2]^{1/2} \times 100$. [c] Goodness-of-fit, GOF = $[\sum w_i(\|\|F_o\| - \|F_c\|\|)^2/(m-n)]^{1/2}$, where m is the number of independent data and n is the number of variable parameters.

Nickel(I) basis functions[36] were used with exponents of 2.0 for the 4s and 4p functions.

Calculations were initially carried out for the Cp ligands, then for the Ni_3Cp_3 and Ni_3S_2 fragments separately, and finally for 1 and 1^+ transformed from appropriate fragments. Further details concerning these calculations are given elsewhere.[19,37]

Crystal Structure Determination of $[Ni_3Cp_3(\mu_3\text{-}S_2)]^+[SbF_6]^-$. Black single crystals were grown from a slowly evaporating CH_2Cl_2 solution under N_2. The crystal selected, an irregularly shaped block of dimensions 0.35 × 0.30 × 0.20 mm, was immobilized with epoxy glue inside an argon-filled Lindemann glass capillary, which was then flame-sealed. Intensity data were collected on a Siemens P3/F diffractometer with graphite-monochromated Mo Kα radiation. Refined lattice constants were determined from a least-squares analysis of 25 well-centered reflections. Axial photographs were taken to confirm the tetragonal lattice lengths and D_{4h} Laue symmetry. All calculations were performed on a DEC MicroVax II system with the SHELXTL-Plus program package. Neutral atomic scattering factors with corrections for anomalous dispersion were used for all non-hydrogen atoms. Crystal data, data collection, and refinement parameters are given in Table III.

The intensities of three standard reflections, which were monitored after every 47 reflections, showed less than ±2% variation during the course of data collection. An empirical absorption correction based on 396 ψ-scan measurements was applied to the intensity data via the XEMP program in the SHELXTL package. Systematic absences of $\{hk0\}$ for $h + k = 2n + 1$ and $\{0kl\}$ for $l = 2n + 1$ uniquely determined the probable tetragonal space group as $P4_2/ncm$ (No. 138, origin choice 2). Conformity of the crystal structure to this centrosymmetric symmetry results in each of the four trinickel cations (1^+) in the unit cell possessing crystallographic C_{2v}-2mm site symmetry, which gives rise to a crystal disorder in the cyclopentadienyl rings (vide infra). Each of the four crystal-ordered $[SbF_6]^-$ anions per unit cell has crystallographic D_2-222 site symmetry, with each of the three pairs of trans fluorine atoms lying on a different 2-fold axis.

Initial positions for the nickel, antimony, and sulfur atoms were found from an interpretation of a Patterson map. The remaining non-hydrogen atoms were located from successive Fourier difference maps coupled with an isotropic least-squares refinement. The Ni_3S_2 core is composed of an isosceles triangle of nickel atoms (with one long and two short edges) capped on each side by a sulfur atom. The apical nickel atom of the isosceles triangle occupies a 4-fold set of special positions with C_{2v}-2mm site symmetry. Of the two mirror planes that intersect at this position, one mirror contains the other two nickel atoms and the second mirror contains the two sulfur atoms. Thus, the crystallographically independent unit for the Ni_3S_2 core of the cation consists of one sulfur and two nickel atoms.

The cyclopentadienyl rings exhibited two different types of crystal disorder.[38] The Cp ligand bonded to the apical nickel atom has a crystallographically imposed rotational disorder due to the 2-fold axis passing through the apical nickel atom. It was modeled in both orientations with the site occupations of the carbon atoms for each orientation fixed at 50%. The two symmetry-related Cp ligands, which are bonded to the other 2-fold-related nickel atoms and which are bisected by the vertical mirror plane that contains the nickel atoms, exhibited a rotational-type crystal disorder. The site occupancy factors of the two 2-fold-related disordered orientations refined to 75% for one ring orientation and 25% for the other.

All non-hydrogen atoms, except for the carbon atoms in the crystal-disordered Cp rings, were refined anisotropically. The hydrogen atoms were fixed in idealized positions during the final stages of refinement with site occupations tied to the associated carbon atom and with their isotropic thermal parameters set at $U = 0.08$ Å^2. The final refinement converged with $R(F) = 4.71\%$, $R_w(F) = 6.14\%$, a goodness-of-fit value (GOF) of 1.36, and a data-to-parameter ratio of 12.9/1 for the 980 independent data with $|F| > 3\sigma(F)$. A final electron-density difference map did not reveal any unusual features. Tables of positional parameters and equivalent isotropic thermal parameters, anisotropic thermal parameters, interatomic distances, bond angles, and idealized parameters for hydrogen atoms are available as supplementary material.

Results and Discussion

Structural Features of $Ni_3Cp_3(\mu_3\text{-}S)_2$ (1). The salient molecular features of 1 were previously reported.[2] The crystal structure of 1 was solved under hexagonal symmetry via an incoherently-twinned model under which the untwinned crystal components were presumed to have $P6_3/m$ symmetry. The resulting crystallographic site symmetry for the Ni_3S_2 core is C_{3h}, which gives rise to an equilateral nickel triangle with a Ni–Ni distance of 2.801(5) Å. The independent triply bridging Ni–S distance is 2.172(6) Å.

Structural Features of $[Ni_3Cp_3(\mu_3\text{-}S)_2]^+[SbF_6]^-$. The tetragonal unit cell of this compound contains four monocations (1^+) and four hexafluoroantimonate anions, which pack under $P4_2/ncm$ symmetry without any abnormally short interionic contacts. The $[SbF_6]^-$ monoanion of crystallographic D_2 site symmetry is constrained to possess an idealized octahedral configuration with cis and

(36) Richardson, R. W.; Nieuport, W. C.; Powell, R. R.; Edgell, W. F. *J. Chem. Phys.* **1962**, *36*, 1057–1061.

(37) North, T. E. Ph.D. Dissertation, University of Wisconsin—Madison, 1989.

(38) Rigid groups for both independent Cp rings were constructed by the same method. The SHELXTL program package did not allow for the inclusion of symmetry-related atoms or crystal-disordered orientations in its rigid-group refinement for cyclopentadienyl rings. With this limitation, it was necessary to create a rigid body for each ring by specifying all distances involved as follows: (1) All C–C bond distances were set to the same value and then allowed to refine collectively tied to a common free variable. (2) The ring diagonal C···C distances were calculated on the basis of the initial value used for the C–C distances and were then allowed to refine as a common free variable. (3) The Ni–C distances were also refined as a common free variable for all the Cp rings. It was necessary to include an "anchor" carbon atom to keep the ring from closing up across the mirror plane. The position of this dummy carbon atom was fixed as the mirror-related atom of the crystallographically independent carbon on the other side of the mirror plane with its site occupation and thermal factors set to zero. The distance between carbon atoms across the mirror could then be included in the constraints of condition 1.

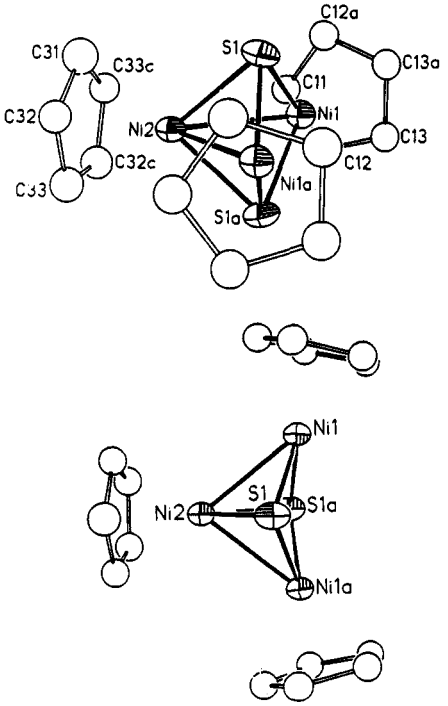

Figure 6. Two views of the 52-electron $[Ni_3Cp_3(\mu_3\text{-}S)_2]^+$ monocation (1^+) with each Cp ring shown in one of its crystal-disordered orientations. Its C_{2v} site symmetry contains an isosceles metal triangle with one nonbonding edge of 3.145(2) Å and two one-electron bonding edges of 2.536(2) Å. The nearly symmetrical capping of the nickel triangle by the apical sulfur atoms is indicated by the two independent Ni(1)–S(1) and Ni(2)–S(1) distances of 2.162(2) and 2.190(2) Å, respectively. Atomic thermal ellipsoids are drawn at the 30% probability level.

trans F–Sb–F bond angles of 90.0 and 180.0°, respectively. The Sb–F distances range from 1.835(7) to 1.853(7) Å with an average value of 1.845 Å. As has been observed in other work in our laboratory, the hexafluoroantimonate anion tends to be better-behaved crystallographically (i.e., ordered instead of disordered) than other counterions such as $[PF_6]^-$ and $[BF_4]^-$.

The $[Ni_3Cp_3(\mu_3\text{-}S)_2]^+$ cation (1^+) possesses crystallographically imposed C_{2v}-2*mm* site symmetry (Figure 6). The trinickel fragment forms an isosceles triangle with two shorter identical edges of 2.536(2) Å and one longer edge of 3.145(2) Å. The mean of the three Ni–Ni distances is 2.739 Å. The nickel triangle is capped by two apical sulfur atoms coordinated to the three nickel atoms. The two independent Ni–S distances are 2.190(2) Å for the S atoms linked to the apical Ni(2) and 2.162(2) Å for the S atoms bonded to Ni(1) and Ni(1a); the weighted mean of 2.17 Å for the six Ni–S bonds is identical to that in **1**. Figure 6 shows the monocation (1^+) with each crystal-disordered Cp ring in its major orientation. The Ni–C(ring) distances refined to a common constrained value of 2.125 Å, while the 15 C–C distances for the cyclopentadienyl rings refined to a common constrained value of 1.43 Å. The intramolecular S···S distance of 2.89 Å is experimentally equivalent to that of 2.90(2) Å in **1**; this unusually short distance suggests the distinct possibility of direct residual S···S interactions in accordance with an approximate normal-coordinate analysis[25] of the two observed Ni–S stretching modes in **1**, indicating coupled vibrations of the two triply bridging sulfur atoms.

Molecular Orbital Bonding Analysis. (a) $Ni_3Cp_3(\mu_3\text{-}S)_2$ (1). Bonding in **1** under idealized D_{3h} geometry for the Ni_3S_2 core can be analyzed from the results of the nonparameterized Fenske–Hall calculation, as summarized in a MO correlation diagram (Figure 7).[39] This diagram reveals that strong interactions between 3d Ni AOs and Cp orbitals of e_1'' symmetry separate the Ni_3Cp_3 fragment orbitals into Ni–Cp bonding and antibonding manifolds and a set of t_{2g}-like nickel 3d orbitals that are essentially Ni–Cp nonbonding. Calculated Ni–Ni interactions are small, as expected for an effectively nonbonding Ni–Ni

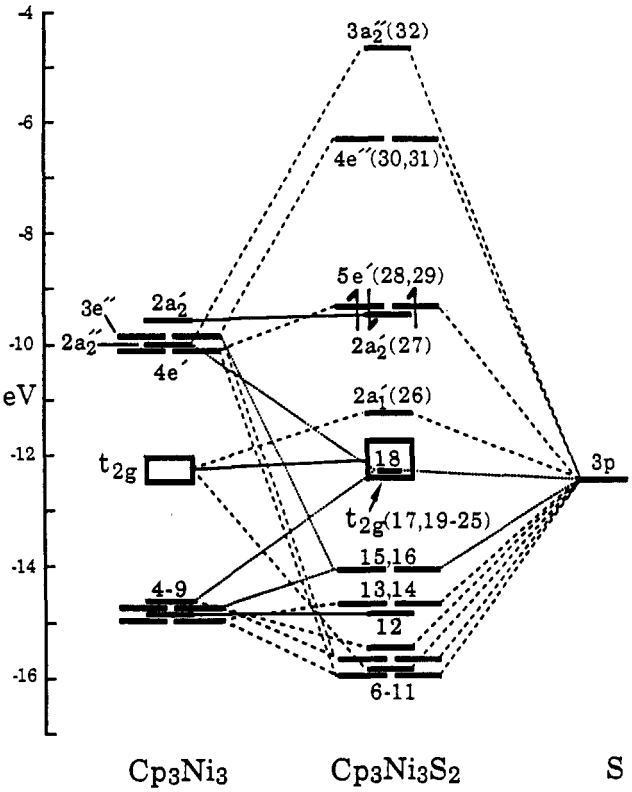

Figure 7. MO correlation diagram for $Ni_3Cp_3(\mu_3\text{-}S)_2$ (**1**) under D_{3h} symmetry. Large dashed lines represent Ni–S bonding and antibonding interactions, smaller dashed lines correspond to Ni–S nonbonding combinations, and solid lines are drawn to orbitals without sulfur contributions. The five valence electrons in **1** occupy the nearly degenerate $2a_2'$ and $5e'$ MOs which are mainly composed of in-plane $3d_{xz}$ Ni AOs. The small energetic separation (ca. 0.12 eV) between the a_2' and e' levels, which are thereby denoted as accidentally degenerate HOMOs, makes it impossible to differentiate between a $^2E'$ ($a_2'^2e'^3$) ground state and a $^2A_2'$ ($e'^4a_2'^1$) ground state; in the case of the former doubly-degenerate ground state, one would expect a small Jahn–Teller induced distortion of the Ni_3S_2 core from a regular trigonal-bipyramidal D_{3h} geometry toward a C_{2v} geometry which presumably would be analogous to that determined for 1^+ (i.e., an isosceles nickel triangle with one longer and two shorter Ni–Ni edges). Particularly noteworthy is that an analysis of the Ni–Ni overlap populations revealed that the e' HOMOs as well as the a_2' HOMO are trimetal-antibonding in agreement with "experimental quantum mechanics".

(39) The orbital designations utilized in the MO calculations of **1** are based upon localized right-handed coordinate axes at each nickel atom being chosen with the *z*-axis pointing to the centroid of the nickel triangle and with the *x*-axis lying in and the *y*-axis perpendicular to the trinickel plane. Of the Ni valence AOs transformed under D_{3h} symmetry into symmetry-adapted combinations, the orbital character of the frontier a_2' and e' MOs may consist of the following nickel valence AOs: a_2' ($3d_{xz}$, $4p_x$); e' ($3d_{z^2}$, $3d_{x^2-y^2}$, $3d_{xz}$, 4s, $4p_x$, $4p_z$). Of the Ni valence orbitals that belong to the e' representation, the $3d_{z^2}$, $3d_{x^2-y^2}$, 4s, and $4p_z$ combinations are trimetal-antibonding while the $3d_{xz}$ and $4p_z$ combinations are trimetal-bonding. For the a_2' representation, both the Ni $3d_{xz}$ and $4p_z$ combinations are trimetal-antibonding.

Table IV. Energies, Percent Compositions, and Ni–Ni Overlap Populations for the Three Frontier Orbitals of $Ni_3Cp_3(\mu_3\text{-}S)_2$ (1) and $[Ni_3Cp_3(\mu_3\text{-}S)_2]^+$ (1^+)

A. $Ni_3Cp_3(\mu_3\text{-}S)_2$ (1) under D_{3h} Symmetry

		% orbital character					Ni–Ni overlap populations[b]	
MO	energy, eV	Ni d_{xz}[a]	Ni $d_{x^2-y^2}$	Ni $4p_x$	Cp e_1''	S 3p	d_{xz}–d_{xz}	total
5e′ (28,29)	–9.35	51	4	3	33	4	+0.005	–0.027
$2a_2'$ (27)	–9.47	60		5	35		–0.012	–0.031

B. $[Ni_3Cp_3(\mu_3\text{-}S)_2]^+$ (1^+) under C_{2v} Symmetry

		% orbital character						Ni–Ni overlap populations[b]	
MO	energy, eV	Ni d_{xz}[a]	Ni d_{z^2}	Ni $d_{x^2-y^2}$	Ni $4p_x$	Cp e_1''	S 3p	d_{xz}–d_{xz}	total
$8a_1$ (29)	–13.42	44	1	4	2	36	10	+0.001	–0.014
$7b_1$ (28)	–13.71	52		3	1	38	3	–0.016	–0.044
$6b_1$ (27)	–14.92	36		4	6	46	2	+0.009	+0.001

[a] The Ni $3d_{xz}$ orbitals lie in the trimetal plane with the z-axis directed toward the centroid of the metal triangle.[15,39] [b] For the partial MO overlap population calculations, each MO is assumed to be occupied by 2 electrons for ease of comparison. The average total Ni–Ni valence overlap population reported for each MO is for all pairs of valence Ni AOs summed over atomic centers and then averaged over the three Ni–Ni interactions.

distance of 2.80 Å. Addition of the two strongly interacting triply bridging sulfur atoms (at the experimental Ni–S distance of 2.17 Å) produces considerable mixing of many of the Ni_3Cp_3 fragment orbitals with the 3p S AOs, while the essentially unmixed 3s S AO remains localized as a lone pair of electrons. The higher-lying trinickel 4s bonding orbital, which is occupied and plays an important role in unligated nickel clusters, lies above the Ni–Cp antibonding manifold and is strongly destabilized by interactions with the triply bridging S atoms so that it does not play a significant role in cluster bonding, as has been observed in other ligated nickel clusters.[19,40]

Here we are particularly concerned with the three occupied frontier orbitals for 1, viz., the near-degenerate $2a_2'$ HOMO (27) and the doubly degenerate 5e′ HOMOs (28,29). Although the Ni–Cp bonding orbitals lying below the t_{2g} set of 3d Ni AOs in the Ni_3Cp_3 fragment interact strongly with the 3p S orbitals, the frontier orbitals do not. Because the 3p S orbitals lack a linear combination of a_2' symmetry, the $2a_2'$ MO remains essentially unchanged in composition and energy from that of the Ni_3Cp_3 fragment. The 5e′ MOs, however, are destabilized by 0.75 eV from the energy level calculated for the Ni_3Cp_3 fragment due to an antibonding interaction with a small 3p S contribution to the predominant in-plane trinickel bonding $3d_{xz}$ and Cp e_1'' contributions. This S contribution to the 5e′ MOs is the determining factor in placing them only 0.12 eV above the $2a_2'$ MO and in making the 5e′ and $2a_2'$ MOs the HOMOs for the cluster under assumed D_{3h} symmetry. The 3e″ Ni_3Cp_3 fragment orbitals, which possess significant out-of-plane $3d_{yz}$ Ni character, are destabilized considerably by interactions with the 3p S orbitals in forming the 4e″ LUMOs (30,31). Orbital compositions, energies, and overlap populations for these frontier orbitals are given in Table IV.

This energy-level ordering, in which two of the five antibonding valence electrons occupy the $2a_2'$ MO and the remaining three electrons the 5e′ MOs, gives rise to an $a_2'^2e'^3$ ground-state electronic configuration. The three-fourths-filled doubly degenerate 5e′ HOMOs are well-separated by ca. 3.0 eV from the doubly degenerate 4e″ LUMOs. Since 1 should then have a degenerate $^2E'$ ground state under assumed D_{3h} symmetry, a first-order Jahn–Teller vibronic distortion should occur. However, since the calculated MO results place the $2a_2'$ MO only 0.12 eV below the 5e′ MOs, one cannot rule out a reversal of these levels to give an $e'^4a_2'^1$ ground-state electronic configuration, which would result in a nondegenerate $^2A_2'$ ground state for 1. Thus, experimental data must be examined to choose between a $^2A_2'$ ground state that should lead to a nondistorted Ni_3S_2 core geometry of pseudo-D_{3h} symmetry and a degenerate $^2E'$ ground state (under D_{3h} symmetry) that should undergo a Jahn–Teller distortion to give a Ni_3S_2 core geometry of pseudo-C_{2v} symmetry with an isosceles nickel triangle. Since the space group $P6_3/m$ of the untwinned crystal component of 1 crystallographically imposes C_{3h}-$3/m$ site symmetry on the independent $Ni_3Cp_3(\mu_3\text{-}S)_2$ molecule, which gives rise to an "averaged structure", it is impossible to infer an electronic configuration from the crystallographic analysis.[41]

Calculations carried out by Rives et al.[15] using the Fenske–Hall method[16] for $Ni_3Cp_3S_2$ under D_{3h} symmetry also predicted trinickel-bonding degenerate e′ HOMOs containing 3 electrons and lying only 0.3 eV above the filled a_2' level. In their calculations, the basis set employed used considerably more diffuse 4s and 4p Ni radial functions and a set of more contracted 3d Ni(II) radial functions. The undesirable consequences of using overly diffuse metal valence s and p AO functions have been discussed by Fenske.[42] The major effect we observe with the updated basis set that employs less diffuse 4s and 4p Ni functions is a reduction of the bonding role of the 4s and 4p Ni AOs and marked enhancement of the interactions of the 3d Ni AOs with the Cp e_1'' orbitals. Of prime interest is that the total Ni–Ni valence overlap populations of the frontier MOs obtained from our calculations indicate that the 5e′ HOMOs of 1 are trimetal-antibonding. Rives et al.[15] had concluded that these e′ MOs are trimetal-bonding on the basis that the in-plane $3d_{xz}$ AOs, which are the major contributors to these degenerate MOs (see Table IV), form a symmetry-adapted trimetal-bonding combination.[39] However, as given in Table IV, the average Ni–Ni $3d_{xz}$–$3d_{xz}$ overlap population has a very small bonding value (+0.005) due to the

(40) (a) Pacchioni, G.; Rösch, N. *Inorg. Chem.* **1990**, *29*, 2901–2908. (b) Rösch, N.; Ackermann, L.; Pacchioni, G. *J. Am. Chem. Soc.* **1992**, *114*, 3549–3555.

(41) The possibility of a highly deformed C_{2v} molecular geometry can be ruled out because the previous crystal structure determination[2] of 1 showed no evidence of a crystal disorder involving an abnormal size or shape of the thermal ellipsoid for the independent nickel atom in the D_{3h} "averaged structure" of the Ni_3S_2 core; the detection of such a crystal disorder would be expected if the resulting 3-fold rotational composite involved the averaging of three highly distorted C_{2v} molecules of 1.

(42) Fenske, R. F. *Pure. Appl. Chem.* **1988**, *60*, 1153–1162.

negligible overlap of the $3d_{xz}$ Ni AOs with one another at the weakly bonding Ni–Ni distance of 2.80 Å. Furthermore, the additional Ni–Ni valence overlap population contributions from the mixed antibonding interactions of the $3d_{x^2-y^2}$, $3d_{z^2}$, 4s, and $4p_z$ Ni AOs with the $3d_{xz}$ Ni AOs gives rise to an average total Ni–Ni overlap population for the 5e′ HOMOs that is antibonding (–0.027). Likewise, the average total Ni–Ni overlap population indicates that the $2a_2'$ HOMO is also trimetal-antibonding, as predicted by Rives et al.[15] on the basis that the major $3d_{xz}$ Ni AO contributors to this MO (see Table IV) form a symmetry-adapted trimetal-antibonding combination.[39] In this case, the contributions due to the other orbitals increase the magnitude of the average Ni–Ni overlap population from –0.012 for the $3d_{xz}$ Ni AOs only to –0.031 for the average total Ni–Ni overlap population for the $2a_2'$ MO.[43,44]

(b) $[Ni_3Cp_3(\mu_3\text{-}S)_2]^+$ (1⁺). The results of a similar MO calculation on 1⁺ under C_{2v} symmetry with the experimentally observed structural parameters (two short bonding Ni–Ni distances of 2.54 Å and one long nonbonding Ni–Ni distance of 3.14 Å) are summarized in the MO correlation diagram shown in Figure 8. Formal oxidation of 1 to 1⁺ stabilizes all levels; the significant shortening of two of the three Ni–Ni distances produces somewhat greater dispersion in all three manifolds of levels (Ni–Cp bonding, Ni–Cp antibonding, and t_{2g}-like), while the lowering of the symmetry from D_{3h} to C_{2v} removes the e′ and e″ orbital degeneracies. The basic electronic structure in the D_{3h} Ni_3Cp_3 fragment of 1, however, is retained in the C_{2v} $[Ni_3Cp_3]^+$ fragment of 1⁺, as is apparent from a comparison of their MO correlation diagrams (Figures 7 and 8). Corresponding orbital interactions of the $[Ni_3Cp_3]^+$ fragment with the triply bridging sulfur atoms in $[Ni_3Cp_3(\mu_3\text{-}S)_2]^+$ (1⁺) give rise to analogous frontier orbitals for the entire cluster, as shown in Figure 8. The $8a_1$ MO (29) and $7b_1$ MO (28), which are slightly destabilized by their 3d Ni orbital interactions with the corresponding 3p S AOs, are separated by only 0.29 eV and hence are presumed to be each occupied by 1 electron. This accidental near-degeneracy, in which both MOs are considered to be the HOMOs, produces a $^3B_1$ ground-state electronic configuration ($b_1^2b_1^1a_1^1$) with two unpaired electrons. The $6b_2$ LUMO (30) and higher-energy $5a_2$ MO (31) and $7b_2$ MO (32) are similarly composed of out-of-plane $3d_{yz}$ Ni AOs that are markedly destabilized by antibonding interactions with the 3p S orbitals. The HOMO–LUMO gap from the upper $8a_1$ HOMO is 1.7 eV. Orbital compositions, energies, and overlap populations for these frontier orbitals are given in Table IV.

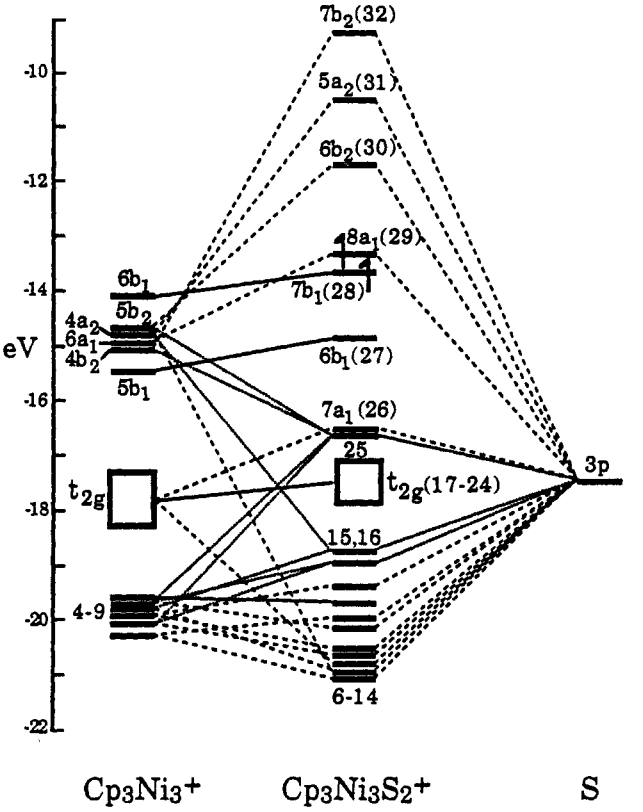

Figure 8. MO correlation diagram for $[Ni_3Cp_3(\mu_3\text{-}S)_2]^+$ (1⁺) for its experimentally determined C_{2v} geometry. Large dashed lines represent Ni–S bonding and antibonding interactions, smaller dashed lines correspond to Ni–S nonbonding combinations, and solid lines are drawn to orbitals without sulfur contributions. This monocation possesses two nearly degenerate $7b_1$ and $8a_1$ MOs, both designated as HOMOs, which contain two unpaired electrons. The experimental data for the 52-electron 1⁺ indicate that its electronic ground state is ^3E ($a_2'^1e'^3$) under D_{3h} symmetry, which results in a Jahn–Teller distortion of the Ni_3S_2 core geometry to give a $^3B_1$ ($b_1^2b_1^1a_1^1$) ground state under C_{2v} symmetry. The MO calculations suggest that the lower fully occupied b_1 level and the upper half-occupied a_1 level arise primarily from the splitting of the e′ level, while the upper half-filled b_1 level originates mainly from the a_2' level.

As indicated in Table IV, both the $8a_1$ and $7b_1$ HOMOs are predicted to be trinickel-antibonding (with average total Ni–Ni overlap populations of –0.014 and –0.044, respectively). Thus, adding 1 electron to either of these trinickel-antibonding HOMOs upon reduction of 1⁺ to 1 should increase the average Ni–Ni bond distance, consistent with the observed increase of 0.06 Å upon reduction. Furthermore, the total Ni–Ni overlap populations for the two HOMOs along the shorter (2.54 Å) edges of the nickel triangle are significantly more antibonding (–0.048 for the $8a_1$ HOMO and –0.064 for the $7b_1$ HOMO) than those for the longer (3.14 Å) edge (+0.003 for the $8a_1$ HOMO and –0.004 for the $7b_1$ HOMO); consequently, the geometrical effect induced by the addition of 1 electron to either of the HOMOs upon reduction of 1⁺ to 1 is predicted to involve a significant lengthening of the two shorter Ni–Ni distances, as is observed experimentally.

(43) It is especially noteworthy that an overlap population analysis of the MOs for 1 obtained by Rives et al.[15] from their basis set would also yield analogous results concerning the trimetal-antibonding character of the e′ and a_2' MOs of 1. Rives et al.[15] did not perform a total Ni–Ni valence overlap population analysis of these frontier MOs acquired from their Fenske–Hall calculations on 1 and related bicapped triangular metal clusters including the 50-electron $Co_3Cp_3(\mu_3\text{-}S)_2$.[7-9,21] Unfortunately, the particular common exponent employed by Rives et al.[15] for the single-ζ 4s and 4p nickel functions in their calculations was not given, and their data output is no longer available. Nevertheless, a smaller exponential coefficient of 1.6 (than that of 2.0 used by us), which would give rise to more diffuse 4s and 4p nickel AOs, was commonly used 10 years ago by the Fenske group.[44] In fact, Rives[44] recently stated that the orbital exponent used for the 4s/4p Ni radial functions in their MO calculations on 1 was probably 1.5 (as originally advocated by Richardson et al.[36]) but certainly no higher than 1.6; his notes also suggest that they used a more contracted 3d Ni(II) basis set with orbital components of 5.75 and 2.20 (in contrast to our 3d Ni(I) basis set with orbital components of 5.75 and 2.00). These particular differences in the nickel radial basis functions are completely consistent with the observed energetic variations of certain MOs in their MO correlation diagram for 1 versus the corresponding ones in our diagram for 1 (Figure 7). Since their chosen basis set consisted of 4s and 4p Ni AOs more diffuse than those currently provided with the latest Fenske–Hall program package utilized by us, it follows that the average Ni–Ni $3d_{xz}$–4s and $3d_{xz}$–$4p_z$ overlap populations for their basis set would give rise to larger negative values characteristic of increased trinickel-antibonding character in the degenerate e′ HOMOsfor 1.

(44) Private communications (1992) from R. F. Fenske and D. R. Kanis to B. Spencer. Private communication (1993) from A. B. Rivers to. L. F. Dahl.

Rives et al.[15] speculated that the expected Jahn–Teller distortion in 1 may be small on account of the long Ni–Ni distances giving rise to weak Ni–Ni interactions. The surprising result of our calculations on 1^+ is that a nearly-degenerate electronic ground state is possible for these systems even after a large observed distortion from D_{3h} symmetry. Thus, 1 may undergo a considerable Jahn–Teller distortion in the solid-state but yet maintain an effectively degenerate ground state at the same time.[41,45]

Structural Comparison of the 52-Electron $[Ni_3Cp_3(\mu_3\text{-}S)_2]^+$ (1^+) with the 53-Electron $Ni_3Cp_3(\mu_3\text{-}S)_2$ (1) and Resulting Bonding Implications. The most striking difference upon oxidation of 1 to 1^+ is observed in the geometry of the triangular nickel framework. Upon conversion of the "averaged" equilateral nickel triangle in 1 into an isosceles nickel triangle in 1^+ with one long and two short sides, the mean Ni–Ni distance decreases by 0.06 Å from 2.80 to 2.74 Å. This significant decrease in the mean Ni–Ni distance is consistent with the removal of a trimetal-antibonding electron from the neutral parent. The mean Ni–S distance remains virtually unchanged upon oxidation of 1 to 1^+.

In relating the geometries of 1 and 1^+, it is important to remember that the observed equilateral nickel triangle in 1 is an averaged structure and that the actual "instantaneous" geometry of 1 is possibly distorted from the crystallographically imposed C_{3h} symmetry toward the C_{2v} geometry observed for 1^+. Nevertheless, the nearly identical mean interatomic distances for all geometric parameters except the mean Ni–Ni distance are strongly suggestive of the fact that the redox-generated change in the geometry of the Ni_3S_2 core upon oxidation mainly involves the trinickel orbital character of the three frontier a_2' and e' MOs (under D_{3h} symmetry). The theoretical results, obtained from calculations by use of the parameter-free Fenske–Hall model, show that the Ni–Cp interactions are antibonding in the HOMOs of 1 and 1^+ and that the HOMOs contain considerable nickel character but little sulfur character. Therefore, the removal of 1 electron from 1 is likely to perturb mainly the Ni–Ni bonds, as is observed here. Unfortunately, the crystal disorder of the Cp ligands in both structures precludes meaningful information being obtained from the mean Ni–C(ring) distances which are experimentally equivalent in 1 and 1^+.

From a valence-bond viewpoint, the 53-electron 1 has a total metal–metal bond order of $^1/_2$ distributed among the three triangular nickel edges. Formation of the 52-electron 1^+ increases the total metal–metal bond order to 1.0. Theoretical investigations of both 1 and 1^+ indicate degeneracy in their HOMOs; in the neutral parent the idealized D_{3h} "averaged structure" for the Ni_3S_2 core gives accidentally degenerate e' and a_2' HOMOs occupied by the five valence electrons, while in 1^+ an accidental near-degeneracy occurs between the a_1 and b_1 HOMOs each occupied by 1 electron under C_{2v} symmetry. It follows that the true Ni_3S_2 core geometry of an individual $Ni_3Cp_3(\mu_3\text{-}S)_2$ molecule (1) has either pseudo-D_{3h} symmetry (consistent with a $^2A_2'$ ground state) or a Jahn–Teller induced C_{2v} distortion (due to a $^2E'$ ground state). A first-order Jahn–Teller vibronic effect is expected to distort the equilateral nickel triangle to an isosceles nickel triangle of C_{2v} geometry with either one shorter and two longer Ni–Ni edges or one longer and two shorter Ni–Ni edges. The fact that the isosceles nickel triangle in 1^+ consists of one long nonbonding Ni···Ni edge and two much shorter bonding Ni–Ni edges provides strong evidence that the nickel triangle in the neutral parent would be similarly distorted if its ground state is $^2E'$ under D_{3h} symmetry.[41]

Spectral–Electrochemical Properties of 1 and 1^+ and Resulting Implications. (a) Cyclic Voltammetric Analysis. CV data for 1 and 1^+ are compared in Table II and Figure 5. The electrochemical behavior of 1 is solvent-dependent, with the degree of reversibility for the redox couples and the appearance of multiple oxidation waves subject to the solvent used. However, two reversible 1-electron transfer steps involving a 0/1+ oxidation wave and a 0/1− reduction wave are invariably exhibited by the CVs in all the solvent systems examined. In acetone solution the oxidation wave occurs at an $E_{1/2}$ value of −0.02 V and the reduction wave at an $E_{1/2}$ value of −0.88 V (vs SCE).

Madach and Vahrenkamp[6] observed similar reversible redox behavior for 1 in benzonitrile solution. In addition to the two reversible processes discussed above, they also reported two irreversible oxidations at +0.94 and +1.15 V. Our CV data for 1 in acetonitrile also exhibit these two irreversible oxidations at similar potentials. In CH_2Cl_2 only the first irreversible oxidation is observed due to the edge of the solvent window being near the anticipated position of the second irreversible oxidation.

As expected, CV data for the 52-electron monocation (1^+) in acetone show two consecutive reversible 1-electron reductions, which correspond to the electrochemical generation of the 53-electron neutral (1) and the 54-electron monoanion. The peak-current ratio of 0.89 for the second reduction couple is significantly less than unity, but both reduction couples still exhibit facile electron-transfer kinetics, as indicated by the independence of the ΔE_p values to changes in scan rate.

A comparison of the redox properties of 1 and 1^+ shows that the $E_{1/2}$ values for the neutral/monocation and the neutral/monoanion waves are identical within 0.01 V for both compounds. This invariance implies that the oxidized form of $Ni_3Cp_3(\mu_3\text{-}S)_2$ produced electrochemically in the CV experiment is the same as the one prepared by chemical means, viz., $[Ni_3Cp_3(\mu_3\text{-}S)_2]^+$ (1^+).

(b) NMR and ESR Analysis. The observation of NMR and ESR signals for paramagnetic species is often mutually exclusive under the same conditions, as is the case here. Line widths associated with the NMR spectra of paramagnetic compounds are generally broadened by the large perturbation in the local magnetic fields introduced by the unpaired electron(s). In order to observe the NMR signal of a paramagnetic species, the electron-spin relaxation time must be sufficiently short to limit the duration of the interaction between the unpaired electron

(45) A similar indication that the e′ HOMOs are *trimetal-antibonding* was obtained from a Co–Co overlap population analysis of the Fenske–Hall calculations subsequently performed (Spencer, B. Unpublished results) on the Cp′-containing 50-electron $Co_3Cp'_3(\mu_3\text{-}S)_2$ (in which a H atom was substituted for the Me substituent on each ring). The molecular parameters utilized in the calculations are based upon the crystallographically determined structure of $Co_3Cp'_3(\mu_3\text{-}S)_2$ which consists of an idealized C_{2v} Co_3S_2 core geometry with one nonbonding (3.19 Å) and two bonding (2.48 Å) Co–Co distances together with six equivalent Co–S distances (2.17 Å).[21] The C_{2v} Co_3S_2 core in this 50-electron cluster is geometrically analogous to the C_{2v} Ni_3S_2 core in the 52-electron 1^+; the geometrical effect of the two fewer trimetal-antibonding electrons on the triangular metal framework in the tricobalt cluster relative to that in the trinickel cluster (1^+) is reflected in each of its two electron-pair bonding edges (BO = 1) being 0.06 Å shorter than each of the two net one-electron bonding edges (BO = $^1/_2$) in 1^+.

and the nucleus.[46] Thus, shorter electron-spin relaxation times favor the observation of NMR signals at the expense of ESR signals.

Proton NMR spectra of 1 and 1^+ show large paramagnetic shifts of the cyclopentadienyl proton resonances from the normal chemical shift value of ~5 ppm to −82 ppm for 1^+ and to −111 ppm for 1. Both of these low-intensity resonances exhibit broad line widths of ca. 1000 Hz. Since the MO calculations indicate that considerable Cp e_1'' orbital character is present in the HOMOs of both 1 and 1^+, it is not surprising that significant unpaired electron-spin density is delocalized from the 3d Ni AOs onto the Cp rings. This suggests that a strong Fermi contact-shift mechanism is operating to generate the large paramagnetic shifts observed for these compounds.[47] To our knowledge, the largest paramagnetic shift previously reported for a triangular metal cluster similar to 1 and 1^+ is exhibited by the 46-electron $Cp^*IrCo_2Cp_2(\mu_3\text{-}CO)_2$ (Cp^* denotes $\eta^5\text{-}C_5Me_5$), where the Cp proton resonance was observed at −46 ppm.[48] The large line widths (viz., 690 and 1300 Hz for 1 and 1^+, respectively) are in accordance with an electron-spin relaxation mechanism that produces an electron-spin-state lifetime sufficiently short to allow the observation of the ^1H NMR signal but not so short as to sufficiently decouple the nucleus from the electron-spin system to give a sharpened line.

ESR spectra are generally well-resolved for species containing one unpaired electron ($S = {}^1/_2$) where electron-spin relaxation is typically inefficient. The absence of an ESR spectrum for 1 in a solvent glass at temperatures ranging from ambient temperature down to 130 K is in agreement with a rapid electron-spin relaxation mechanism associated with near-degenerate ground states.[49]

(c) Electronic Spectral Analysis. UV–vis spectra of 1 and 1^+ as the $[SbF_6]^-$ salt in CH_2Cl_2 solution each exhibit two bands of interest in the visible and near-UV region. These similar bands account for both compounds being a reddish-brown color in solution. Band A in 1 appears at 396 nm and in 1^+ undergoes a small blue shift to 382 nm. Band B in 1 is observed in the near-UV at 272 nm and in 1^+ also undergoes a blue shift to 264 nm. In addition, the spectrum of 1^+ exhibits two equally-spaced shoulders positioned at λ values approximately ±60 nm relative to λ_{max} of band A (Figure 4).

In spite of the fact that 1^+ has been shown to possess a solid-state C_{2v} geometry and its neutral parent (1) may be similarly distorted (to a much smaller extent) from a 3-fold-averaged molecular configuration, room-temperature visible spectra of 1 and 1^+ in solution are most conveniently rationalized under an assumed D_{3h} geometry for both species. Approximate molecular orbital calculations for 1 and 1^+ under D_{3h} symmetry are in good agreement with the observed electronic transitions. The frontier orbitals of 1 under D_{3h} symmetry and assignments for bands A and B are shown in Figure 9. Band A is assigned as an electronic transition between the degenerate e′ HOMOs and the degenerate e″ LUMOs, while band B

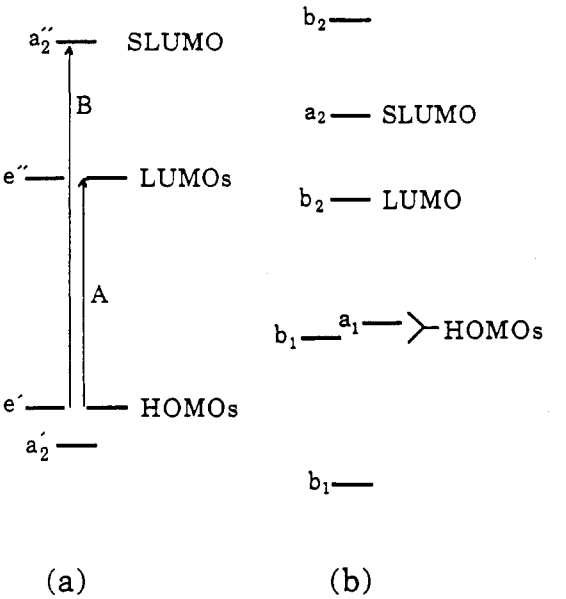

Figure 9. Comparison of (a) the frontier orbitals of $Ni_3Cp_3(\mu_3\text{-}S)_2$ and $[Ni_3Cp_3(\mu_3\text{-}S)_2]^+$ under D_{3h} symmetry with the observed electronic transitions assigned as bands A and B and (b) the corresponding frontier orbitals under C_{2v} symmetry.

Table V. Observed and Calculated Electronic Transition Energies for $Ni_3Cp_3(\mu_3\text{-}S)_2$ (1) and $[Ni_3Cp_3(\mu_3\text{-}S)_2]^+$ (1^+)

	obsd, eV (nm)		calcd, eV (nm)	
species	band A	band B	band A	band B
1	3.13 (396)	4.56 (272)	2.98 (416)	4.72 (263)
1^+	3.25 (382)	4.70 (264)	3.14 (395)	4.86 (255)
Δ	+0.12	+0.14	+0.16	+0.14

is assigned as a transition from the same HOMOs to the a_2'' SLUMO (i.e., second lowest unoccupied MO). For the monocation (1^+) which possesses a similar set of frontier orbitals under assumed D_{3h} symmetry, the calculated energies for bands A and B are larger than those in 1. As shown in Table V, the calculated transition energies are in good agreement with the observed transitions. The calculations are also in accordance with the observed blue shifts for both bands.

Under C_{2v} symmetry the degeneracies of the HOMOs and the LUMOs are broken to give the frontier orbitals shown in Figure 8. The energies of the transitions associated with bands A and B are considerably smaller, and no blue shift is predicted for the monocation (1^+). However, a molecular distortion to C_{2v} symmetry, which presumably would produce additional bands, is consistent with the shoulders observed on either side of band B in 1^+.

(d) Mass Spectral Analysis. Both positive- and negative-ion LD/FT mass spectra of 1 exhibit the molecular ion as the most intense peak (m/z 435); the isotopic distribution pattern was found to be entirely consistent with the compound's composition. Although the positive-ion spectrum displayed only one other major peak corresponding to the $[NiCp_2]^+$ fragment (m/z 188), the negative-ion spectrum gave a number of other relatively abundant peaks which suggest the occurrence of different fragmentation patterns for the parent ion. Fragment ion peaks corresponding to the successive loss of two sulfur atoms are observed at m/z 403 and 370, respectively; the loss of the second sulfur is accompanied by the simultaneous loss of a ring hydrogen. The presence of another

(46) Swift, T. J. In *NMR of Paramagnetic Molecules*; La Mar, G. N., Horrocks, W. DeW., Holm, R. H., Eds.; Academic Press: New York, 1973; Chapter 2.
(47) Horrocks, W. DeW.; In *NMR of Paramagnetic Molecules*; La Mar, G. N., Horrocks, W. DeW., Holm, R. H., Eds.; Academic Press: New York, 1973; Chapter 4.
(48) Herrmann, W. A.; Barnes, C. E.; Zahn, T.; Ziegler, M. L. *Organometallics* **1985**, *4*, 172–180.
(49) Figgis, B. N. *Introduction to Ligand Fields*; Interscience: New York, 1967; Chapter 11.

fragmentation sequence is indicated by the $[M - Cp]^-$ and $[M - 2Cp]^-$ ion peaks corresponding to the successive loss of two Cp rings from the parent ion; the $[M - Cp]^-$ ion also gives a set of isotopic peaks centered at m/z 370. The calculated isotopic pattern indicates that the corresponding peaks for this $[M - Cp]^-$ ion should occur at m/z 0.1 higher than those for the $[M - 2S - H]^-$ ion, and both closely spaced isotopic sets of peaks were resolved in the mass spectrum. The $[NiCp_2]^-$ ion fragment is barely observable in the negative-ion spectrum, as would be expected for this highly unstable negative ion.

The positive-ion LD/FT mass spectrum of $1^+[SbF_6]^-$ exhibited only one major peak corresponding to the $[NiCp_2]^+$ ion, while the negative-ion LD/FT spectrum only displayed three major peaks characteristic of successive loss of two fluorine atoms from the $[SbF_6]^-$ counterion.

(e) Analysis of Magnetic Susceptibilities. Both the neutral $Ni_3Cp_3(\mu_3\text{-}S)_2$ (1) and its monocation (1^+) as the $[SbF_6]^-$ salt exhibit temperature-dependent magnetic behavior in the solid state. Figure 1 shows the temperature dependence of the effective magnetic moments (μ_{eff}) that were obtained for 1 from three independently prepared samples. The general trend observed is a gradually decreasing moment, which rapidly falls from approximately 2.4 μ_B at 298 K to 1.0 μ_B below 50 K. The average room-temperature (298 K) moment of 2.4 ± 0.1 μ_B is larger than the spin-only moment of 1.73 μ_B expected for one unpaired electron. The temperature dependence of the moment varies to a small extent from sample to sample. Similar behavior has been observed for materials with highly anisotropic magnetic properties such as the ferrocenium salts.[50] Figure 2 shows a similar temperature dependence of the effective magnetic moments (μ_{eff}) obtained for the $[SbF_6]^-$ salt of 1^+ from three samples. The average room-temperature moment of 2.84 ± 0.14 μ_B agrees well with the spin-only value of 2.83 μ_B expected for a triplet state. However, the effective moments also diminish to a low-temperature limit of approximately 1.0 μ_B.

Figure 3 compares the temperature dependence of the inverse of the susceptibility (χ^{-1}) for typical measurements of 1 and the $[SbF_6]^-$ salt of 1^+. The plot for the neutral 1 deviates from linearity in the high-temperature region where the χ^{-1} curve will be most sensitive to a temperature-independent paramagnetic (TIP) contribution. Attempts to model the temperature-dependent magnetic data for 1 as a singlet state in thermal equilibrium with a triplet excited state by use of the Bleaney–Bowers equation[51] were not successful. Correcting for these TIP contributions with empirically derived constants ranging from 700 to 1400 × 10^{-6} emu/mol gives linear χ^{-1} vs T plots. A fit of the corrected data from the three samples to the Curie–Weiss expression, $\chi = C/(T - \theta)$, gives an average μ_{eff} of 1.88 ± 0.33 μ_B which compares favorably with the spin-only value. The Weiss constants (θ) obtained vary from −2.5 to −14 K.

A representative χ^{-1} vs T plot for the $[SbF_6]^-$ salt of the monocation (1^+) in Figure 3 shows that χ^{-1} is linear in T at temperatures in the region above 100 K. Deviation from Curie behavior occurs in the low-temperature region where the χ^{-1} vs T plot bends downward to superimpose the plot exhibited by 1. A fit of the data above 100 K (with no TIP corrections) from the three samples to the Curie expression gave an average μ_{eff} of 3.21 ± 0.28 μ_B. The calculated Weiss constants are considerably more negative than those obtained for 1, with θ values ranging from −52 to −138 K. The negative θ values obtained for 1 and 1^+ suggest that intermolecular antiferromagnetic interactions are present which are in accordance with similar decreases in the temperature-dependent magnetic moments exhibited by both compounds at low temperature.

The effective magnetic moments of 1 and 1^+ calculated from measurements of the magnetic susceptibilities in solution via the Evans NMR method are consistent with spin-only magnetism. A μ_{eff} of 1.7 ± 0.3 μ_B was reported[2] for 1 in solution, and our measurements of the magnetic susceptibility of 1^+ in solution give an effective magnetic moment of 2.72 ± 0.01 μ_B. Four measurements made over the temperature range from 298 to 205 K indicate that the moment of 1^+ is temperature-independent. A plot of the inverse molar susceptibility versus temperature for these four measurements is linear, indicating that 1^+ obeys the Curie–Weiss law in solution. The magnetic moment calculated from the χ^{-1} vs T plot is 2.66 μ_B and θ = +2 K.

The low-temperature magnetic behavior of both 1 and the $[SbF_6]^-$ salt of 1^+ in the solid state is consistent in both compounds with an antiferromagnetic coupling of electron spins that partially quenches the magnetic moment at low temperatures. No ordering temperature is observed for either compound, but plots of μ_{eff} vs T show a rapid downturn at approximately 50 K. For 1, which has an odd number of electrons, no other explanation accounts for the magnetic moment falling below the spin-only value at low temperatures. The adherence of the solution susceptibilities of 1^+ to the Curie–Weiss law with a Weiss constant near zero indicates that the antiferromagnetic behavior observed in the solid state is likewise due to intermolecular interactions.

Our theoretical investigations of these compounds indicate that the unpaired electron(s) in the HOMOs are partially delocalized from the triangular nickel fragment onto the Cp rings and to a much smaller extent also onto the sulfur atoms. Antiferromagnetic ordering of the electron spins is thus expected to arise through intermolecular interactions between these atoms. An antiferromagnetic exchange mechanism must arise via the closest intermolecular contacts of 1 and 1^+. The shortest intermolecular distances in 1 are 3.42 Å between carbon atoms in two Cp rings and 3.70 Å between the Cp carbon atoms and the triply bridging sulfur atom. In the $[SbF_6]^-$ salt of 1^+ the shortest intermolecular C···S distance is 3.57 Å, while the shortest C···C distance between two Cp rings is 3.84 Å. For both compounds, the intermolecular S···S distances are considerably larger.

Opposing the effects of antiferromagnetic coupling in 1 is a second-order Zeeman effect associated with near-degenerate ground states that are split by spin–orbit coupling.[52] If the ground state couples with higher-lying excited states that have $\Delta E \gg kT$, a temperature-independent paramagnetism (TIP) is observed. The successful application of large TIP corrections to the magnetic data to give linear χ^{-1} vs T plots and spin-only

(50) (a) Miller, J. S.; Calabrese, J. C.; Harlow, R. L.; Dixon, D. A.; Zhang, J. H.; Reiff, W. M.; Chittipeddi, S.; Selover, M. A.; Epstein, A. J. *J. Am. Chem. Soc.* **1990**, *112*, 5496–5506. (b) Miller, J. S.; Epstein, A. J.; Reiff, W. M. *Science* **1988**, *240*, 40–47.

(51) Carlin, R. L. *Magnetochemistry*; Springer-Verlag: New York, 1986; p 75 ff.

(52) Figgis, B. N. *Introduction to Ligand Fields*; Interscience: New York, 1967; Chapter 10.

moments supports the assignment of a second-order Zeeman effect. The MO calculations on 1 and 1^+ show that degenerate or near-degenerate ground states occur for 1 in either a D_{3h} geometry or a Jahn–Teller-distorted C_{2v} geometry.

Structural-Bonding Comparison of $Ni_3Cp_3(\mu_3\text{-}S)_2$ (1) with $[Ni_3(PEt_3)_6(\mu_3\text{-}S)_2]^{2+}$ and Other $[M_3L_6(\mu_3\text{-}S)_2]^{2+}$-Type Complexes. The geometry and electronic configuration of 1 can be related to those of the $[M_3L_6(\mu_3\text{-}S)_2]^{2+}$-type complexes (M = Ni, Pd, Pt; L = phosphine), which are exemplified by $[Ni_3(PEt_3)_6(\mu_3\text{-}S)_2]^{2+}$,[53] $[Pd_3(PMe_3)_6(\mu_3\text{-}S)_2]^{2+}$,[54] and $[Pt_3(PMe_2Ph)_6(\mu_3\text{-}S)_2]^{2+}$.[55] Each of these trimetal–disulfide complexes possesses a pseudo-D_{3h} geometry consisting of a trigonal-bipyramidal M_3S_2 core with each M atom additionally linked to two phosphine ligands in a square-planar coordination. The resulting overall architecture may be described as three square-planar *cis*-MP_2S_2 moieties that are symmetry-related by a pseudo 3-fold axis passing through the two common triply bridging S atoms. An electron count of 48 (instead of the usual value of 54) for each of these $[M_3L_6(\mu_3\text{-}S)_2]^{2+}$ complexes is consistent with the trimetal moiety possessing no metal–metal bonds (in accordance with the observed M···M nonbonding distances) because each square-planar d^8 M(II) metal conforms to a 16-electron count rather than the normal 18-electron closed-shell electronic configuration.

If each Cp^- anion in 1 is viewed to be a 4-electron-donating bidentate ligand occupying two square-planar coordination sites (instead of a 6-electron-donating tridentate ligand), it follows that 1 is structurally analogous to the $[M_3L_6(\mu_3\text{-}S)_2]^{2+}$-type cluster in containing three square-planar *cis*-MCp_2S_2 moieties. In this case, 1 then bookkeeps as a 47-electron trimetal system, which is 1 electron short of having three nonbonding diamagnetic d^8 Ni(II) atoms. Particularly noteworthy is that the original MO calculations by Rives et al.[15] and those presented herein show that the three out-of-plane trinickel e″ and a_2'' frontier MOs are unoccupied; these empty symmetry-adapted orbitals correspond to each nickel atom having a vacant $3d_{yz}$ AO which resembles the high-energy empty $3d_{x^2-y^2}$ AO of a conventional square-planar d^8 Ni(II) configuration (for which the x- and y-axes are directed toward the four ligands). Besides providing credence in the observed energy-level ordering of the frontier MOs in the MO diagram of $Ni_3Cp_3(\mu_3\text{-}S)_2$ (Figure 7), this correlation points to the close electronic relationship between $Ni_3Cp_3(\mu_3\text{-}S)_2$ and the $[M_3L_6(\mu_3\text{-}S)_2]^{2+}$-type complexes. Nevertheless, we prefer to describe the electronic configuration of 1 as a 53-electron trinickel cluster with each Cp^- anion formally depicted as a 6-electron-donating tridentate ligand.

Summary

An X-ray crystallographic study of $[Ni_3Cp_3(\mu_3\text{-}S)_2]^+[SbF_6]^-$ reveals that the monocation (1^+) of crystallographic C_{2v}-2*mm* site symmetry consists of an isosceles nickel triangle with one nonbonding edge of 3.145(2) Å and two bonding edges of 2.536(2) Å. 1^+ is an unprecedented example of a bicapped triangular metal cluster with 52 valence electrons. From a valence-bond viewpoint the resulting total net metal–metal bond order of 1.0 must be equally distributed between the two Ni–Ni bonding edges to give a localized bond order of 0.5 for each edge corresponding to a net 1-electron metal–metal bond. The weighted mean Ni–Ni distance of 2.74 Å in 1^+ is 0.06 Å shorter than the Ni–Ni distance of 2.801(5) Å for the C_{3h} averaged structure in $Ni_3Cp_3(\mu_3\text{-}S)_2$ (1). This decrease in the Ni–Ni distance is consistent with the removal of a trinickel-antibonding electron from 1.

Comparative MO calculations carried out on 1 and 1^+ with the Fenske–Hall model are correlated with the experimental data. Our MO results for 1 differ somewhat from those of a previous Fenske–Hall MO calculation reported by Rives et al.[15] due to our use of an updated atomic basis set involving less diffuse 4s and 4p and more diffuse 3d Ni AOs. Nevertheless, our energy-level ordering of the three frontier MOs occupied by the five valence electrons in 1 is virtually identical, with the energy level of the a_2' HOMO being only 0.12 eV below that of the degenerate 5e′ HOMOs under D_{3h} symmetry; hence, we concur with Rives et al.[15] that one cannot theoretically distinguish whether the Ni_3S_2 core in 1 has pseudo-D_{3h} symmetry consistent with a $^2A_2'$ ($a_2'^1e'^4$) ground state or a Jahn–Teller induced C_{2v} geometrical distortion due to a $^2E'$ ($a_2'^2e'^3$) ground state. Of prime interest, however, is that our calculations on both 1 and 1^+ indicate (in direct opposition to the previous interpretation made by Rives et al.[15]) that the e′ HOMOs as well as the a_2' HOMO of 1 (and the corresponding two HOMOs of 1^+) are trimetal-antibonding, in agreement with our earlier experimentally-based bonding model[2,11] (and subsequent electron-counting schemes[12]) for 1 and related electron-rich triangular metal clusters possessing valence electron counts in excess of 48. The solid-state C_{2v} geometry of 1^+ supports the premise that if 1 has a $^2E'$ ground state under pseudo-D_{3h} symmetry the observed solid-state C_{3h} averaged structure of the neutral parent (1) is then a 3-fold composite of a C_{2v} geometry composed of a similarly deformed isosceles nickel triangle. The fact that the size, shape, and orientation of the thermal ellipsoid for the crystallographically independent nickel atom in 1 does not exhibit any evidence of a crystal disorder strongly indicates that the observed averaged structure of 1 cannot be a 3-fold composite of a highly distorted isosceles nickel triangle. The MO calculations for the experimentally determined C_{2v} Ni_3S_2 core geometry of 1^+ also revealed a near-degeneracy of the two half-occupied a_1 and b_1 HOMOs; the resulting ground state for the four valence electrons in 1^+ is $^3B_1$ ($b_1^2b_1^1a_1^1$), which under D_{3h} symmetry would correspond to $^3E'$ ($a_2'^1e'^3$) in order to produce the observed large Jahn–Teller induced C_{2v} geometrical distortion of the Ni_3S_2 core.

Magnetic susceptibility measurements show complex temperature-dependent behaviors for both 1 and 1^+. The observed magnetic moments at room temperature for the neutral parent (1) correspond to one unpaired electron in the solid state, in agreement with measurements performed in solution. The observed magnetic moments at room temperature for the monocation (1^+) in both the solid state and solution correspond to two unpaired electrons. These experimental results at room temperature are completely consistent with the number of unpaired electrons predicted

(53) (a) Ghilardi, C. A.; Midollini, S.; Sacconi, L. *Inorg. Chim. Acta* **1978**, *31*, L431–L432. (b) Cecconi, F.; Ghilardi, C. A.; Midollini, S. *Inorg. Chem.* **1983**, *22*, 3802–3808.

(54) Werner, H.; Bertleff, W.; Schubert, U. *Inorg. Chim. Acta* **1980**, *43*, 199–204.

(55) (a) Bushnell, G. W.; Dixon, K. R.; Ono, R.; Pidcock, A. *Can. J. Chem.* **1984**, *62*, 696–701. (b) Chatt, J.; Mingos, D. M. P. *J. Chem. Soc. A* **1970**, 1243–1245.

by the Fenske–Hall MO model for both 1 and 1^+. This correlation is most gratifying in justifying the validity of this widely utilized nonparameterized MO model which has had a major impact in providing meaningful insight concerning redox-generated variations in geometric/electronic structures of transition-metal clusters.

Acknowledgements. We gratefully appreciate the financial support of this research by the National Science Foundation. We thank Professor Mary-Ann Pearsall (then, UW—Madison; now, Drew University, Madison, NJ) for her assistance in obtaining UV–vis spectra. We are especially indebted to Dr. Joel Miller and Mr. Scott McLean (Central Research and Development Department, Experimental Station, E. I. du Pont de Nemours and Co., Inc., Wilmington, DE 19880-0328) for obtaining the variable-temperature solid-state magnetic susceptibility data. We also gratefully acknowledge Dr. Robert Weller (then, EXTREL FTMS; now, Westinghouse Savannah River Co.; Aiken, SC) for obtaining mass spectral data and EXTREL FTMS (6416 Schroeder Rd., Madison, WI 53711) for the use of a FTMS-2000 mass spectrometer.

Supplementary Material Available: Tables of atomic positions, anisotropic thermal displacement coefficients, interatomic distances, and bond angles for non-hydrogen atoms and idealized atomic and isotropic thermal parameters for hydrogen atoms of $[Ni_3Cp_3(\mu_3\text{-}S)_2]^+[SbF_6]^-$ (5 pages). Ordering information is given on any current masthead page.

OM920609B